COMPARISON AND OPTIMIZATION OF MULTIPLE INTERACTING CONTINUA (MINC) MODEL PARAMETERS

A THESIS SUBMITTED TO
THE GRADUATE SCHOOL OF NATURAL AND APPLIED SCIENCES
OF
MIDDLE EAST TECHNICAL UNIVERSITY

BY

EBRU BERNA DEMİR

IN PARTIAL FULFILLMENT OF THE REQUIREMENTS
FOR
THE DEGREE OF MASTER OF SCIENCE
IN
PETROLEUM AND NATURAL GAS ENGINEERING

SEPTEMBER 2023

Approval of the thesis:

COMPARISON AND OPTIMIZATION OF MULTIPLE INTERACTING CONTINUA (MINC) MODEL PARAMETERS

submitted by **EBRU BERNA DEMİR** in partial fulfillment of the requirements for the degree of **Master of Science** i**n Petroleum and Natural Gas Engineering, Middle East Technical University** by,

Prof. Dr. Halil Kalıpçılar
Dean, Graduate School of **Natural and Applied Sciences** _____

Assist. Prof. Dr. İsmail Durgut
Head of the Department, **Petroleum and Natural Gas Eng.** _____

Assist. Prof. Dr. Mehmet Onur Doğan
Supervisor, **Petroleum and Natural Gas Eng., METU** _____

Examining Committee Members:

Assoc. Prof. Dr. Çağlar Sınayuç
Petroleum and Natural Gas Eng., METU _____

Assist. Prof. Dr. Mehmet Onur Doğan
Petroleum and Natural Gas Eng., METU _____

Assist. Prof. Dr. Doruk Alp
Petroleum and Natural Gas Eng., METU NCC _____

Date: 05.09.2023

I hereby declare that all information in this document has been obtained and presented in accordance with academic rules and ethical conduct. I also declare that, as required by these rules and conduct, I have fully cited and referenced all material and results that are not original to this work.

Name Last Name : Ebru Berna Demir

Signature :

ABSTRACT

COMPARISON AND OPTIMIZATION OF MULTIPLE INTERACTING CONTINUA (MINC) MODEL PARAMETERS

Demir, Ebru Berna
Master of Science, Petroleum and Natural Gas Engineering
Supervisor: Assist. Prof. Dr. Mehmet Onur Doğan

September 2023, 94 pages

In recent years, unconventional reservoirs have become a new trend in the oil industry because of the decrease in conventional hydrocarbon reserves. One of the commonly encountered types is shale gas reservoirs, where gas production can be enhanced with fracturing. Reservoir simulation has been significantly important to have future predictions for a long time. Understanding the transport processes in naturally fractured reservoirs is challenging compared to unfractured reservoirs. While matrix has extremely low permeability, fracture has extremely high permeability. Mainly two numerical conceptual models can be applied to this type of fractured reservoirs which are Continuum Fracture Model (CFM) and Discrete (DFM) Fracture Model (DFM). CFM requires calculation of some specific transfer parameters (shape factors, volume fractions etc.) implicitly to interpret transport processes between the matrix continua and fracture continuum. DFM requires huge computation power and cost to analyze fractures explicitly. Conductivity and connectivity of fractures are taken into account individually. This thesis focuses on parameter estimation of Multiple Interacting Continua (MINC) one of CFM models by taking DFM as a reference solution. The objective function for parameter

estimation is mass storage rate deviation from DFM model simulated on a Bristol geometry, located along the Bristol Channel coast in the United Kingdom. The computation cost of MINC model is more efficient compared to DFM model and requires fewer pre-processing efforts for geometry discretization. Volume fractions can be calculated on a representative part of the domain and can be used for the hole reservoir as long as the reservoir has the same fracture distribution as the representative part of the field.

Keywords: Continuum Fracture Modeling, Discrete Fracture Network, Multiple Interacting Continua, Upscaling, Volume Fractions

ÖZ

ÇOKLU ETKİLEŞİMLİ SÜREKLİLİK (ÇES) MODELİ İÇİN PARAMETRE KIYASLAMASI VE OPTİMİZASYONU

Demir, Ebru Berna
Yüksek Lisans, Petrol ve Doğal Gaz Mühendisliği
Tez Yöneticisi: Dr. Öğretim Üyesi Mehmet Onur Doğan

Eylül 2023, 94 sayfa

Petrol sektöründe konvansiyonel rezervlerin azalmasıyla beraber, son yıllarda ankonvansiyonel rezervlere yönelim arttı. Sıkça karşılaşılan tiplerden biri doğal olarak çatlaklar gösterebilen kaya gazı rezervuarlarıdır. Rezervuar simülasyonları geleceğe dair öngörü sahibi olmak için, uzun süredir, çok büyük bir öneme sahiptir. Çatlaklı olmayan rezervuarlarla göre, doğal çatlaklı rezervuarlarda taşınım proseslerini anlamak daha zordur. Matrisin çok düşük bir geçirgenliği varken, çatlakların geçirgenliği çok yüksektir. Bu tarz çatlaklı rezervuarları modellemek için Birleşik Çatlaklı Model (BÇM) ve Ayrık Çatlaklı Model (AÇM) olmak üzere iki ana kavramsal modelleme yöntemi kullanılabilir. BÇM, matris ve çatlaklar arasındaki taşınım prosesini anlamak için, dolaylı olarak hesaplanıp elde edilen bazı temel parametreler (şekil faktörü, hacim fraksiyonu vb.) gerektirir. AÇM ise çatlakları doğrudan analiz etmek için devasa hesaplama gücü ve maliyete ihtiyaç duyar. Bu tez, BÇM modellerinden biri olan çoklu etkileşimli süreklilik (ÇES) modeli için gerekli olan parametreleri AÇM modeli referans çözüm alarak hesaplamaktadır. Parametre tahmini için, kütle birikim hızının, Birleşik Krallık'ta Bristol Kanalı sahilinde bulunan Bristol geometrinin AÇM modelinden sapması objektif fonksiyondur. ÇES modelinin hesaplama maliyeti AÇM ile karşılaştırıldığı zaman daha avantajlıdır ve geometri detaylarının işlenmesi için gerekli çaba daha azdır. Hacim fraksiyonları belirli bir alanın temsili bir parçası üzerinde

hesaplanabilir. Tüm saha, temsili alanla aynı çatlak dağılımına sahipse, bulunan parametreler belirli bir alanın temsili bir parçası üzerinde hesaplanıp tüm saha için kullanılabilir.

Anahtar Kelimeler: Sürekli Çatlak Modelleme, Ayrık Çatlak Ağ Modellemme, Çoklu Etkileşimli Süreklilik, Üst Ölçeklendirme, Hacim Fraksiyonları

To My Father

ACKNOWLEDGMENTS

I would like to express my sincerest acknowledgments to my supervisor, Assist. Prof. Dr. Mehmet Onur Doğan, for his endless patience, guidance, encouragement and unwavering support throughout the research process. He was always helpful and illuminated the way for my research, even during my most challenging times.

I would like to thank Assoc. Prof. Dr. Çağlar Sınayuç for his constructive criticism and professional demeanor and for being a part of my thesis defense committee. In addition, I would also like to extend my thanks to the other committee member, Assist. Prof. Dr. Doruk Alp, for his contribution and invaluable comments.

I would like to express my heartfelt gratitude to my husband, Barış Demir, for his unwavering support, understanding, and love throughout this rigorous research period and my entire life. His steadfast presence has been a source of great hope and strength, especially during difficult times.

TABLE OF CONTENTS

LIST OF TABLES

TABLES

LIST OF FIGURES

FIGURES

LIST OF SYMBOLS

SYMBOLS

a	absorption coefficient, s/m^2
A	cross-sectional area of the pipe, m^2
$A_{f,m_{DFM}}$	total interface area between matrix and fractures in DFM model, m^2
$A_{f,m_{MINC}}$	total interface area between matrix and fractures in MINC model, m^2
$A_{i,j}$	interface area, m^2
$A_{j,j+1}$	interface areas between continuum *i* and *j,* m^2
c	diffusion coefficient, s
c_f^i	concentration of the i^{th} gas component
d_a	damping term, s^2/m^2
$d_{i,j}$	nodal distance, m
$d_{j,j+1}$	distance between j^{th} and $j+1^{th}$ nodes, m
$d_{x_{frac}}$	fracture spacing, m
e_a	mass coefficient term, s^3/m^2
f_1	fracture volume fraction
f_i	source term, kg/(m^{3}s)
f_j	volume fraction of j^{th} volume element
q	source or sink term, kg/(m^{3}s)
k	permeability, m^2
k_f	fracture permeability, m^2
$k_{m_{DFM}}$	matrix permeability of DFM model, m^2
$k_{m_{MINC}}$	matrix permeability of MINC model, m^2
L	distance of pipe, m
$\bar{p}^k$	average pressure of cell k, Pa
$\bar{p}^l$	average pressure of cell l, Pa

p	pressure, Pa
$\bar{p}$	average pressure, Pa
Q	volumetric flow rate, m^3/s
$\bar{Q}$	volumetric flow rate at mean pressure, m^3/s
Q_f	fracture flow rate, m^3/s
$Q^{k,l}$	flow rate through interface, m^3/s
t	time, s
u	average fracture velocity, m/s
u_y	velocity in y direction, m/s
u_f	average gas velocity through fracture, m/s
V	volume, m^3
V_0	total volume of volume element, m^3
V_j	volume of j^{th} volume element, m^3
V_m	total matrix volume of volume element, m^3
V_n	total volume of volume element, m^3
x	half of fracture aperture, m
x_a	actual data
α	conservative flux convection in x & y direction, s/m
β	convection coefficient in x & y direction, s/m
γ	conservative flux source in x & y direction, $kg/(m^2s)$
δ	fracture aperture, m
μ	viscosity of fluid, Ns/m^2
ρ	density of fluid, kg/m^3
$\bar{\rho}$	average density, kg/m^3
σ	shape factor, $1/m^2$
σ	number of elementary units
$\tau^{k,l}$	transmissibility between cell *k* & cell *l*
ϕ	porosity

CHAPTER 1

INTRODUCTION

Unconventional reservoirs are in high demand due to the decrease in conventional reservoirs. Naturally fractured reservoirs (NFR) represent one of the most complex unconventional reservoir types. These reservoirs formed as a result of fragmentation during tectonic movements of massive rock blocks. Consequently, fractures are distributed randomly throughout the matrix.

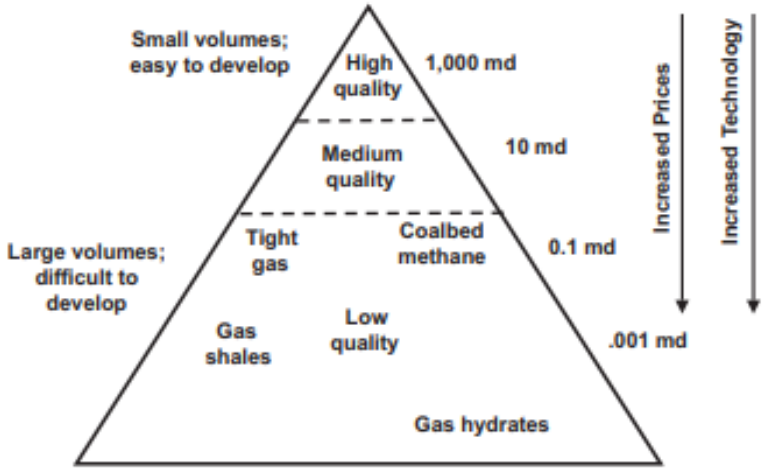

Figure 1.1 The resource pyramid (Holditch, 2006)

Gray (1977) introduced a resource pyramid, which illustrates that high-permeability reservoirs occupy the top tier, while low-permeability reservoirs are situated at the bottom. Conventional reservoirs, characterized by their high quality, small volumes, and ease of development, have become scarce. In contrast, low-quality unconventional reservoirs boast significant volumes but demand more advanced production technologies. This decrease in high-quality conventional reservoirs has

led to a growing demand for tight reservoirs, particularly shale gas reservoirs. Furthermore, the resource pyramid in Figure 1.1, emphasizes the need for improved technology and development strategies to enhance recovery from unconventional reservoirs.

Naturally fractured reservoirs have a common point, low permeability, and high heterogeneity. Therefore, modeling fluid flow in shale gas reservoirs is more complex and requires more attention than in conventional reservoirs.

Although fractures have a small portion of the reservoir, fluid transportation mainly occurs within the fractures. However, the reservoir is primarily made up of matrix. Fractures have low storage capacity and high permeability, while matrices have high storage capacity and low permeability. This difference causes discontinuity between the matrix and fractures. Thus, these heterogeneities make modeling fluid flow and transport processes inside the fractured reservoirs challenging.

Creating a model that represents the matrix and the fractures properly is a crucial job. There are several methods, such as Continuum Fracture Model (CFM) (i.e., multiple interacting continua, dual porosity- dual permeability models), Discrete Fracture Model (DFM), and hybrid model. DFM models are well-known as representative models for the fractured reservoirs since they analyze each fracture individually. This advantage brings some drawbacks, which are extremely long computation time and high cost.

One of CFM models is Multiple Interacting Continua (MINC) was originally designed by Pruess and Narasimhan (1982). MINC models are based on a straightforward nested volume element approach. Increasing the number of volume elements improves the model's representation of the reservoir. Each volume element is associated with a volume fraction, and the sum of all volume fractions must equal to 1. Volume fraction represents the proportion of one nested element to the total

volume of nested elements. Every homogeneously fractured reservoir has its own unique volume fractions. Determining these distinctive volume fractions is essential for effectively applying the MINC model concept.

In this study, the naturally fractured Bristol geometry, located along the Bristol Channel coast in the United Kingdom, is employed. One of the study's objectives is to compare five different MINC methods. Additionally, parameter optimization is undertaken to create the most representative MINC model. Two optimization problems are addressed in this thesis. The first challenge involves determining upscaled matrix permeability for a continuum model assembled alongside the DFM model. The second optimization is to determine volume fractions for a ten-interacting continua model, using the DFM model as a reference.

CHAPTER 2

LITERATURE REVIEW

Fractured reservoirs can exhibit both primary permeability, often referred to as matrix permeability, and secondary permeability, known as fracture permeability, simultaneously. Matrix permeability develops during the sedimentation process, whereas fracture permeability emerges after post-sedimentary rock processes, such as compaction or cementation, have taken place. The geological complexity of such rocks arises from the coexistence of these two distinct permeabilities. To model reservoirs with this dual permeability characteristic, researchers commonly employ continuum and discrete fracture models.

2.1 Continuum Approach

This approach incorporates the behavior of fractures implicitly, where matrix and fractures are treated as a continuous medium rather than discrete entities. Several continuum approach models exist, each requiring specific parameters such as shape factors and volume fractions to be defined. Small-scale fractures are typically identified in regions where the rock is poorly fractured, while large-scale fractures are recognized in domains where fracture-dominated flow prevails. It's important to note that continuum models are more commonly applicable to small-scale fractured reservoirs rather than those with larger-scale fractures (Ouenes & Hartley, 2000).

2.1.1 Dual Porosity Single Permeability (DPSP) Model

Dual porosity (DP) was initially introduced by Barenblatt et al. in 1960 with the intention of studying fluid seepage in fissured systems. In their early work, there was

an assumption that the system was homogeneous. However, it was later realized that fissure systems exhibit significantly higher permeability compared to porous media.

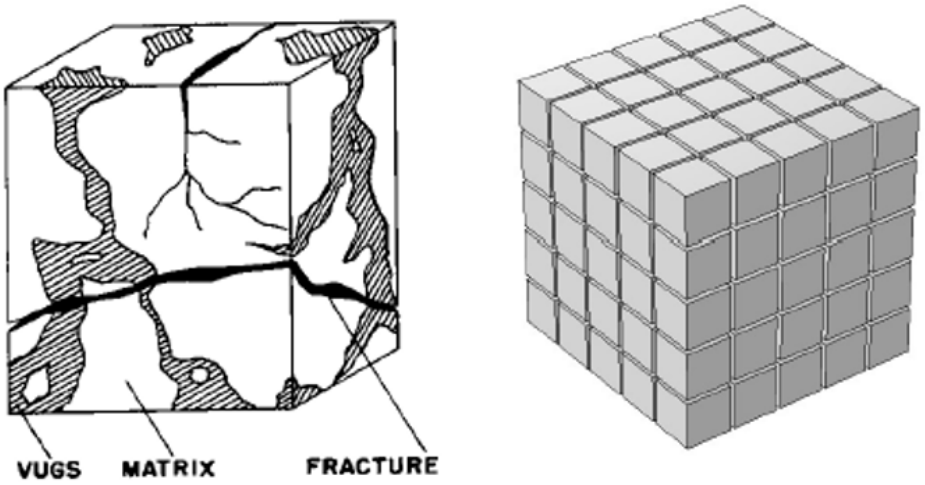

Figure 2.1 Idealization of heterogeneous porous medium- Actual Reservoir and Model Reservoir (Warren & Root, 1963)

The DP model in Figure 2.1 was initially introduced by Warren & Root (1963). In this model, primary porosity is intergranular and develops during the deposition and lithification processes, while secondary porosity is foramenular and arises after fracturing, jointing, or infilling through precipitation processes, as outlined by Warren & Root (1963). This model acknowledges the transport of fluids between fractures and between fractures and matrices, as illustrated in Figure 2.2. However, it does not account for fluid flow from one matrix to another, as matrix continua are not interconnected.

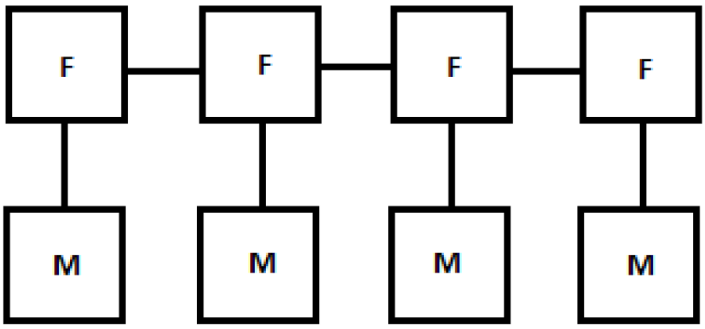

Figure 2.2 Dual porosity single permeability flow schematic diagram

To apply DP model effectively, it is essential for the flow within the reservoir to reach a quasi-steady state condition, as highlighted by Warren & Root(1963). Consequently, it is important to note that if the reservoir does not attain a pseudo-steady state condition, the use of DP model can lead to inaccurate estimations, particularly in the early-time region, as observed by Jiang & Younis (2016).

2.1.1.1 Dual Porosity-Shape Factors

In 1963, Warren & Root introduced DP model to the petroleum industry, introducing a novel concept, shape factor parameter of a transfer function (as depicted in Figure 2.3). To elucidate fluid flow from matrix to fractures transfer function is introduced. Transfer function is function of matrix permeability, viscosity of the fluid, the difference between matrix and fracture pressure and shape factor. Table 2.1 provides a summary of three distinct shape factor constants, denoted as σL^2 (where σ represents the shape factor and L is the fracture spacing), for each dimension. These shape factor constants are derived from solutions of the diffusivity equation under the assumption of constant fracture pressure. They are applied for analytical or numerical modeling in either pseudo-steady state or transient flow regimes. Transient flow refers to a non-steady state condition in which flow properties, such as temperature and pressure, change with time. On the other hand, pseudo-steady

state, also known as quasi-steady state, assumes conditions where flow properties remain nearly constant over time.

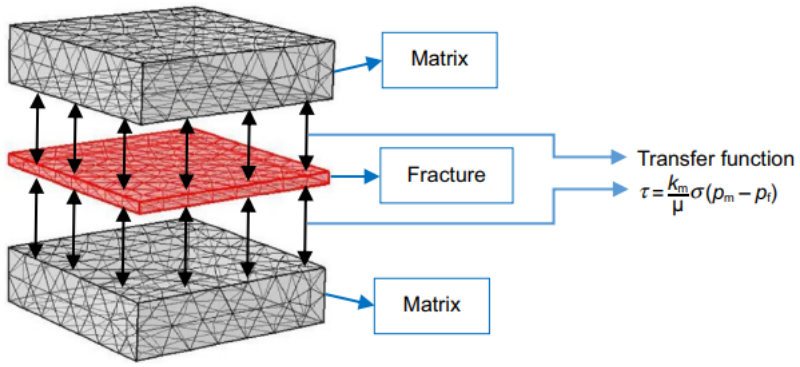

Figure 2.3 Schematic of the transfer function between the matrix and the fractures (Rostami et al., 2020)

Coats (1999), Kazemi and Gilman (1993) and Lim and Aziz (1995), introduced different shape factors even for a single-phase flow by analytical approach. Kazemi et al. (1976) applied the first numerical method for a single-phase flow under pseudo-steady state flow conditions. Bourbiaux et al. (1999), Sarda et al. (2002), Penuela et al. (2002) and Mora and Wattenbarger (2006) applied numerical approaches in order to decide shape factors; while Bourbiaux et al. (1999) decided it for transient flow regime, the others completed under pseudo-steady state conditions. Hassanzadeh and Pooladi-Darvish (2006) have used Laplace domain analytical solutions of the diffusivity equation. Furthermore, they concluded that shape factors are a function of time and fracture pressure and change with time. Rostami et al. (2020) have studied shape factors for multidimensional irregular bodies by a numerical approach for a single-phase flow.

Table 2.1 Summary of Shape Factor Constants (Rostami et al., 2020)

References	$N=1$	$N=2$	$N=3$	Approach	PSS/Transient
Warren and Root (1963)	12	32	60	Numerical	PSS
Kazemi et al. (1976)	4	8	12	Numerical	PSS
Peaceman (1976)	12	14.23	16.53	Numerical	PSS
Thomas et al. (1983)	–	–	25	Numerical	Transient
Ueda et al. (1989)	8	24	–	Numerical	PSS
Coats (1989)	12	28.45	49.58	Analytical	PSS
de Swaan (1990)	12	–	60	Numerical	PSS
Zimmerman et al. (1993)	9.87	19.74	29.61	Numerical	PSS
Kazemi and Gilman (1993)	9.87	19.74	29.61	Analytical	Transient
Chang (1993)	9.87	19.74	29.61	Numerical	PSS
Lim and Aziz (1995)	9.87	19.74	29.61	Analytical	Transient
Quintard and Whitaker (1996)	12	28.4	49.6	Averaging	Transient
Bourbiaux et al. (1999)	–	20	–	Numerical	PSS
Noetinger and Estebenet (2000)	11.5	27.1	–	Random walk technique	Transient
Sarda et al. (2001)	8	24	48	Numerical	Transient
Penuela et al. (2002a, b)	9.87	–	–	Numerical	Transient
Hassanzadeh and Pooladi-Darvish (2006)	9.87	18.2	25.56	Analytical	PSS
Mora and Wattenbarger (2009)	9.87	18.17	25.67	Numerical	PSS
Hassanzadeh et al. (2009) (constant rate)	12	25.13	38.9	Analytical	PSS

Eventually, mass transfer from matrix to fractures is in direct proportion to shape factors. There is no unique solution to calculate shape factors. The correct shape factor value must be decided for each type of flow regime and also the geometry of the fractured porous media.

2.1.2 Dual Porosity Dual Permeability (DPDP) Model

DPDP models are created where the flow exists not only between fractures but also in the matrix. A computer model, considering not only matrix permeability but also discrete fracture network, was developed by Hull and Clemo (1987).

The representation of fluid flow in the reservoir is shown in the Figure 2.4. Usually, matrix permeability is significantly lower than fractured permeability.. DPDP modeling can pose challenges and require substantial computational power, making it a less common choice for naturally fractured reservoirs, especially when simpler models may suffice.

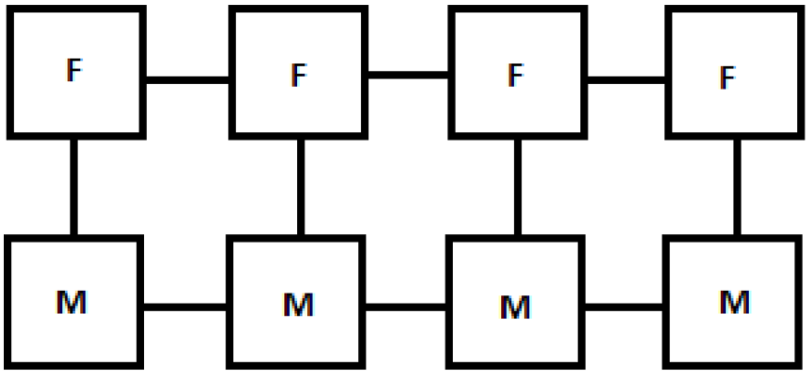

Figure 2.4 Dual porosity double permeability flow schematic diagram

2.1.3 Multiple Interacting Continua (MINC) Model

Like dual porosity models, matrix has low permeability and high storage capacity, while fractures have high permeability and low storage capacity for multiple interacting continua (MINC) concept. MINC models are based on dual porosity concept, but the matrix media is subdivided into nested blocks. In dual porosity approach, analytical approximations are available only for regularly shaped matrix blocks such as slabs, cubes, or spheres while there is no regular shape limitation in MINC model approach. MINC was originally designed by Pruess and Narasimhan (1982) and developed by Pruess and Narasimhan (1985) at the Lawrence Berkeley Laboratory to model interconnected fractures where the flow mainly occurs.

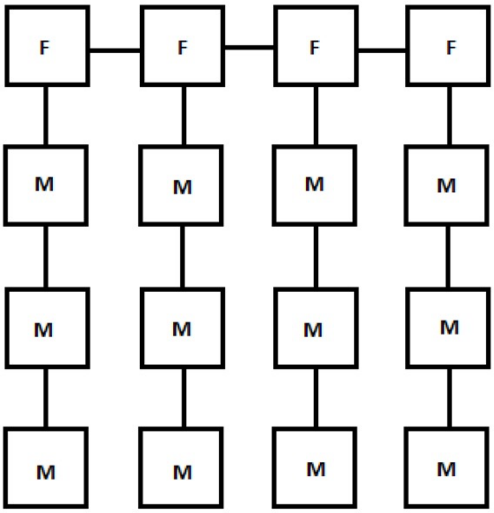

Figure 2.5 MINC model flow schematic diagram

Long-term transient flow regime is experienced due to the minimal matrix permeability (Jiang & Younis, 2016; Mayerhofer et al., 2006). Therefore, high resolution is required around the fractures where thermodynamics alters vigorously to analyze pressure gradients and mass exchange (Pruess & Narasimhan, 1985).

One of the main advantages and superiority to dual-porosity models is that they can be applicable to transient problems where a quasi-steady state condition is not compulsory. There is only one condition to apply MINC model that fractures must be interconnected sufficiently so that fractured network is a continuum (Farah et al., 2016; Pruess, 1992).

Instead of partial differential equations, finite difference method is easily used to designate the distances between each nested block with the help of mass and energy equations (Narasimhan & Witherspoon, 1978; Pruess, 1992).

2.2 Discrete Fracture Approach

This model considers the individual effect of each fracture on fluid flow. Fracture coordinates, porosity, permeability (in x, y, z direction), compressibility, and matrix-fracture exchange mass are defined in this model individually (Lei et al., 2017). In order to create a proper discrete fracture model, fracture characteristics, fracture aperture, orientation, and dip angle of fractures and their distributions are needed.

While modeling fractured reservoirs, discrete fracture models are options for dual continuum models (Karimi-Fard et al., 2006). It is true that DFM can involve significant computational costs while they possess a distinct advantage over Continuum Fracture Models (CFM) in their ability to directly simulate fluid flow interactions between fractures and matrices, as well as between fractures and between matrices themselves. Unlike CFM, DFM does not require the use of transfer functions. This direct representation of fluid flow is a notable superiority of DFM in reservoir modeling (Egya, 2018).

There are three different types of DFM models:

- Discrete Single Fracture model
- Discrete Fracture Network model
- Discrete Fracture Matrix model

2.2.1 Discrete Single Fracture Model

Discrete Single Fracture model operates on the premise that flow and transport occur within a single, well-defined fracture or a few such fractures (Billaux et al., 1989; Tsang & Tsang, 1987). This concept simplifies the representation of rough wall surfaces by invoking the idea of parallel plates, originally introduced by

Lomize (1951). It achieves this by eliminating macro or micro roughness, allowing for a more tractable approach to modeling fluid flow and transport.

Although fracture aperture width and orientation and roughness are changing locally, parallel plates model assumes constant aperture for single fractures (Tatomir, 2012).

2.2.2 Discrete Fracture Network Model

Matrix is accepted as impermeable, so the flow mainly occurs in the interconnected fractures. Tsang and Tsang (1987) introduced a model which represents DFN, existence of one-dimensional fluid flow in a fractured 2–3-dimensional rock. An example of discrete fracture model of a large scaled naturally fractured reservoirs is shown in Figure 2.6.

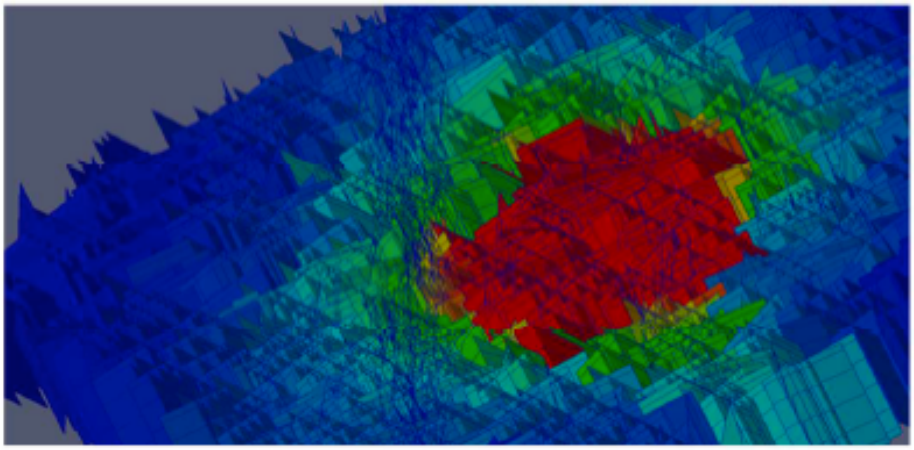

Figure 2.6 A 3D large fracture network with an irregular fracture distribution (Farah et al., 2016)

2.2.3 Discrete Fracture Matrix Model

Fractures exchange fluid with the surrounding matrix in this model besides the flow in the fracture network. Since fracture is the main flow pathway due to its high permeability while matrix mainly acts as a storage unit due to its low permeability, flow mainly occurs in the fracture network and there is no fluid exchange between matrices usually. Therefore, this model type is not frequently applied.

2.3 Hybrid Model Approach

Both continuum and discrete models can be adapted for naturally fractured reservoirs where fluid flow primarily occurs within fractures while the matrix plays a minor role in fluid transfer. Table 2.2 presents a comparison of continuum models and discrete models. In continuum models, the level of resolution is typically low, implying that these models favor simplified representations of fractures, coarser grids, straightforward meshing, and lower demands on computational resources such as processing power and memory. In contrast, discrete models are characterized by high resolution, signifying the need for detailed fracture representations, finer grids, complex meshing, and a substantial demand for computational resources. Continuum approaches offer advantages in terms of computation time and cost, as fractures are analyzed implicitly through the introduction of effective parameters. However, a notable drawback of continuum models is their inability to consider the impact of disconnected fractures (Kuchuk et al., 2014). In contrast, discrete models analyze the effects of each fracture individually. Nevertheless, their primary limitation is their applicability to field-scale problems due to the high computational cost and time required (Xue et al., 2019). In other words, discrete models are typically preferred for small-scale problems characterized by relatively small fracture dimensions or less densely distributed fractures within the rock formation. These limitations have led to the development of a hybrid model that combines elements of both continuum and

discrete approaches, addressing the need for a higher resolution in modeling fractured reservoirs.

Table 2.2 Comparison of Continuum and Discrete Models (Modified from Egya D. (2018))

Criteria	Continuum Models	Discrete Models
Level of resolution	low	high
Computation time	low	high (days)
Computational cost	low	high
Scale in applicability	large	small
Fracture representation	implicit	explicit
Effective properties	required (shape factor, volume fractions etc.)	-
Upscaling	required	-

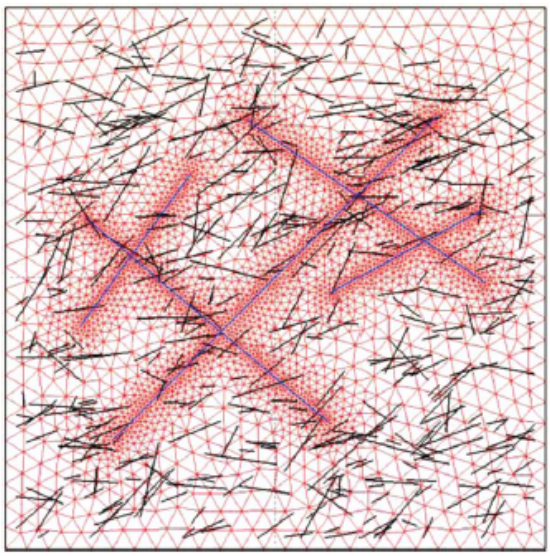

Figure 2.7 Schematic of unstructured gridding and embedded-fracture network in the hybrid model (Jiang & Younis, 2016)

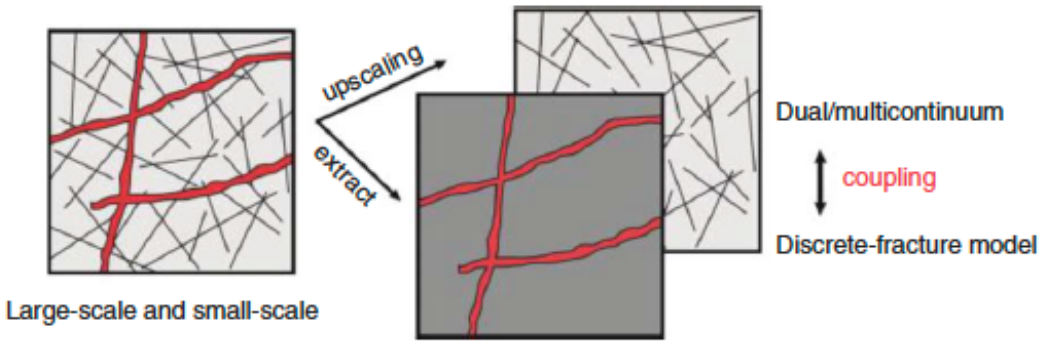

Figure 2.8 Schematic illustrating a hybrid modeling approach for small- (black lines) and large-scale (red lines) fractures (Jiang & Younis, 2016)

A hybrid model, as developed by Lee et al. (2001), addresses the modeling of fractures of varying sizes. Embedded discrete fracture models (EDFM), which is exemplified in Figure 2.7, were introduced, by Li and Lee (2008). These models employ a hybrid finite volume method to simulate naturally fractured reservoirs at a field scale. Figure 2.8 explains that large scale fractures are modeled with discrete fracture network whereas small scale fractures are modeled via dual continuum approach (Moinfar et al., 2013; Wu et al., 2014).

Hybrid model is advantageous due to the lower computation time and good resolution of created models (Jiang & Younis, 2016; Ren et al., 2017; Xue et al., 2019; Yang et al., 2018).

CHAPTER 3

STATEMENT OF PROBLEM

Modeling fluid flow and transport processes in fractured reservoirs is a challenging task. CFM models are well-priced and time-saving while DFM is more accurate and representative of a field. However, DFM has two significant drawbacks: expensive computational time and excessive data requirements. The main objective of this study is to develop a realistic and representative model for the complex Bristol geometry, using CFMs. CMF models require well-connected fracture distributions and some non-unique, applicable parameters, which have previously been calculated for simple reservoir models. Bristol geometry, meeting MINC condition that fractures are sufficiently interconnected, is modeled with discrete fracture network method on COMSOL Multiphysics finite element method software. Five different MINC models are formed to compare with DFM. The last one, which gives the most similar results to DFM, is created by optimizing specific parameters (e.g., volume fractions). Mass storage vs. time graph of the last MINC model and DFM are matched. The error between the optimized MINC and DFM is calculated by mean squared error calculation method. The previously created model, optimized MINC, represents the best DFM model. Modeling fractures using MINC model helps to simulate the Bristol geometry in a brief time with the least effort.

CHAPTER 4

METHODOLOGY

This chapter explains how to properly gather data to create DFM and MINC model of an unstructured geometry using the COMSOL Multiphysics program. In addition, which principles applied to create models are discussed in detail.

It should be noted that this model specifically considers the transport of a single-phase fluid, methane, within the fractured porous medium. This model can be likened to a shale gas reservoir, which may be naturally fractured or subjected to hydraulic fracturing processes. That's because these reservoirs have a very low matrix permeability and consist of huge amounts of methane with a little percentage of other hydrocarbons. Produced methane rarely has small percentages of carbon dioxide, nitrogen, ethane, or maybe propane in real life (Ahmed, 2010).

COMSOL is employed to numerically solve Darcy's flow equations while considering changes in fluid properties. Methane, selected as the ideal gas for the models in COMSOL, introduces the need to derive Darcy's law due to methane's compressibility. Fracture permeability equations are derived from the Navier-Stokes equation, and partial differential equations are formulated for both models. MINC concept is elucidated in detail, and the calculation of corresponding parameters for a 2D model is demonstrated. Furthermore, parameters from DFM model are upscaled for MINC models. Upscaling means that certain characteristics or properties derived or determined from DFM model are adjusted or transformed to be compatible with and applicable to the MINC models.

Initially, the matrix permeability is optimized for MINC models, and subsequently, volume fractions of nested volume elements are optimized to have the same mass

storage vs. time graph as much as possible with DFM. The workflow diagram is summarized as follows:

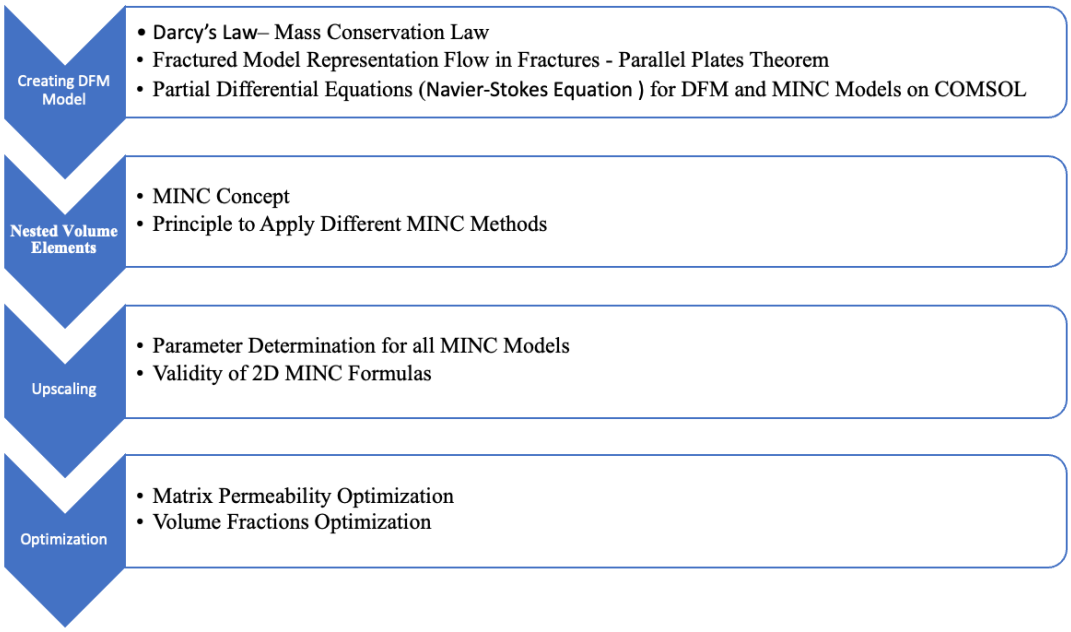

Figure 4.1 Workflow diagram

4.1 Fractured Model Representation - Fluid Flow Characteristics

It can be challenging even for methane molecules to move within shale gas reservoirs due to the limited pore spaces. However, fractures caused by natural earth movement and overlying deposits allow the reservoir components (oil, gas, water) to flow. These fractures cause high discontinuity within the rock. Eventually, these heterogeneities require determination of not only matrix properties but also fracture properties.

4.1.1 Darcy's Law

Permeability is one of the most significant parameters in porous media. The ability of fluid to flow in a porous rock is called permeability and explained by Darcy's law.

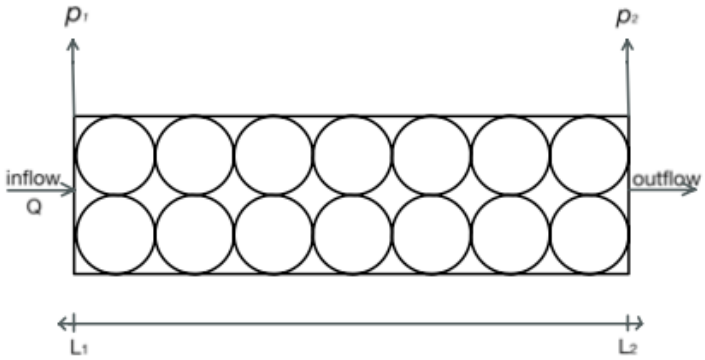

Figure 4.2 Darcy's Law horizontal flow representation

When isotropic rock is subjected to pressure gradient between two points Darcy's equation comes into play:

$$Q\int_{L_1}^{L_2} dL = -\frac{k}{\mu}A\int_{p_1}^{p_2} d\mathrm{p} \tag{4.1}$$

$$Q(L_1 - L_2) = -\frac{k}{\mu}A(p_2 - p_1) \tag{4.2}$$

$$\frac{Q}{A} = -\frac{k}{\mu}\frac{\Delta p}{\Delta L} \tag{4.3}$$

Where Q is the flow rate, A is cross-sectional area of the pipe in Figure 4.2, L is the distance where the pressure gradient observed, k is the permeability, μ is the viscosity of the fluid, p_1 is the left boundary pressure and p_2 is the right boundary pressure.

Henry Darcy created this formula for the fluids with the assumption under slightly compressible single-phase flow within porous media. However, in the model it must be noted that methane is a compressible fluid. Thus, density of the fluid changes with

time because it is function of pressure and temperature. In this condition, the volumetric flow rate is changing with time in contrast mass flow rate is not changing. Therefore, the equation is rearranged:

$$\rho_1 Q_1 = \rho_2 Q_2 = \rho_b Q_b = \rho Q \tag{4.4}$$

P is the density of the fluid, b is the base condition.

Boyle's law is applied under isothermal condition:

$$p_1 V_1 = p_2 V_2 = p_b V_b = pV \tag{4.5}$$

or volume flow rate can be written instead of volume:

$$p_1 Q_1 = p_2 Q_2 = p_b Q_b = pQ \tag{4.6}$$

When eqn 4.5 and eqn 4.6 is combined:

$$\frac{p_b Q_b}{\rho_b Q_b} = \frac{pQ}{\rho Q} \tag{4.7}$$

Density becomes:

$$\rho = \rho_b \left(\frac{p}{p_b}\right) \tag{4.8}$$

The new Darcy's equation is derived as followed:

$$\rho \frac{Q}{A} = -\frac{k}{\mu} \rho \frac{dp}{dx} \tag{4.9}$$

$$\rho_b \frac{Q_b}{A} = -\frac{k}{\mu}\left(\rho_b \frac{p}{p_b}\right)\frac{dp}{dx} \tag{4.10}$$

Base density terms are cancelled:

$$\frac{p_b Q_b}{A} = -\frac{k}{\mu} p \frac{dp}{dx} \tag{4.11}$$

Integrating $\frac{\mathrm{dp}}{\mathrm{dx}}$:

$$\frac{p_b Q_b}{A} L = \frac{k}{\mu}\frac{(p_1^2 - p_2^2)}{2} \tag{4.12}$$

So that base volume flow rate will be equal to:

$$Q_b = \frac{kA}{2\mu L}\frac{(p_1^2 - p_2^2)}{p_b} \tag{4.13}$$

Solving for the flow rate:

$$Q_b p_b = \frac{kA}{2\mu L}(p_1^2 - p_2^2) \tag{4.14}$$

Note that, arithmetic average pressure is equal to:

$$\bar{p} = \frac{p_1 + p_2}{2} \tag{4.15}$$

$$p_b Q_b = \bar{p}\bar{Q} \tag{4.16}$$

$$Q_b P_b = \bar{p}\bar{Q} = \frac{kA}{2\mu L}(p_1^2 - p_2^2) \tag{4.17}$$

$$\frac{p_1 + p_2}{2}\bar{Q} = \frac{kA}{2\mu L}(p_1^2 - p_2^2) \tag{4.18}$$

$$\frac{p_1 + p_2}{2}\bar{Q} = \frac{kA}{2\mu L}(p_1 - p_2)(p_1 + p_2) \tag{4.19}$$

When $(\mathrm{p}_1 + \mathrm{p}_2)$ terms are cancelled, the volumetric flow rate at mean pressure ($\overline{\mathrm{Q}}$) for ideal gasses can be calculated from the following equation:

$$\bar{Q} = \frac{kA}{\mu}\frac{(p_1 - p_2)}{L} \tag{4.20}$$

Methane is identified as ideal gas for the models in COMSOL where the equation 4.20 can be used to find the flow rate at mean pressure.

4.1.1.1 Darcy's Law in Fractures - Parallel Plates Theorem

During constant source of methane injection to the DFM model, fracture aperture can exchange during time due to the compressibility of the gas. Hence, the mass balance equation for fracture apertures get starts (Liu et al., 2019):

$$\frac{\partial}{\partial t}\left(\delta c_f^i \phi\right) = -\frac{\partial}{\partial l}\left(c_f^i \mathrm{u}_f \delta\right) \tag{4.21}$$

ϕ is the porosity of the fracture system, δ is the fracture aperture, c^i_f is the concentration of the i^{th} gas component in the fractures (where there is only methane concentration), u_f is the average gas velocity through the fracture.

$$\delta \frac{\partial}{\partial t}\left(c_f^i \phi\right) + c_f^i \phi \frac{\partial \delta}{\partial t} = -\frac{\partial}{\partial t}\left(c_f^i u_f \delta\right) \tag{4.22}$$

The temporal derivative of fracture aperture $\frac{\partial \delta}{\partial t}$ can be negligible (Chen et al., 2020).

Mass balance equation for fractures in porous media becomes:

$$\delta \frac{\partial}{\partial t}\left(c_f^i \phi\right) = -\frac{\partial}{\partial l}\left(c_f^i u_f \delta\right) \tag{4.23}$$

Fluid flow in fractures resembles the flow in parallel plates Figure 4.3. In addition to mass conservation, momentum conservation is also required by Navier-Stokes equation applicable for which fluid flows in two parallel plates.

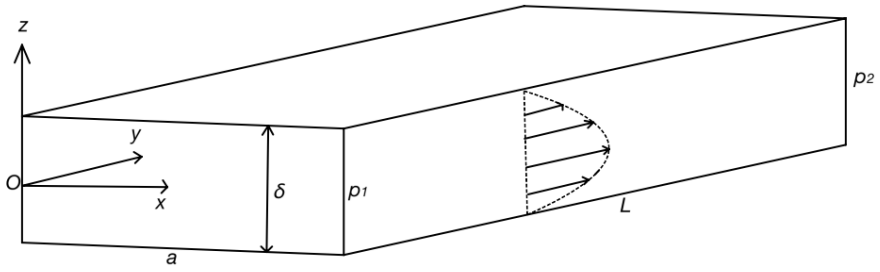

Figure 4.3 Fluid flow between parallel plates

$$\left[\rho_f \frac{\partial u}{\partial t} + u \cdot \nabla u\right] = -\nabla p + \nabla \cdot [\mu(\nabla u + u\nabla)] + \rho_f g \tag{4.24}$$

The cubic law is derived from the fundamental principles of Darcy's law and the Navier-Stokes equation. This relationship serves as a simplification that is particularly relevant for describing laminar flow in porous media, especially in scenarios involving compressible gases, as encountered in certain natural gas reservoirs. The well-known cubic law for a single-phase compressible gas flow is:

$$\rho\left(\frac{\partial u}{\partial t}+u\nabla u\right)=-\nabla p+\mu\nabla^2 u \tag{4.25}$$

It is assumed that fluid flow within fractures follows Poiseuille's law, which subsequently leads to the well-known cubic law which describes laminar flow within the porous medium governing the overall flow rate (Chen et al., 2020). Like cubic law, Poiseuille's law provides the relationship between flow rate, pressure drop, fluid viscosity and pipe dimensions. However, it is applicable to laminar flow of Newtonian fluids through cylindrical pipes or tubes. Also, the flow regime is assumed as steady state so $\frac{\partial \mathrm{u}}{\partial \mathrm{t}}$ is neglected. Boundary conditions are accepted as no slip conditions which emphasizes that the velocity of the fluid must equal to the velocity of the plate at anywhere on the boundary (Batchelor, 1967; Zimmerman et al., 1994). In this condition, inertia forces are very small compared to viscous forces. Additionally, when fractures are oriented horizontally gravitational effects can be minimal and neglected.

The combination of Equation 4.23 obeying the cubic law, the Navier-Stokes equation with the given assumptions becomes:

$$\frac{p_1-p_2}{L}+\mu\frac{\partial^2 u_y}{\partial^2 z^2}=0 \tag{4.26}$$

There is only one flow direction, y direction in Figure 4.3. Integrating the equation by applying boundary condition, velocity profile:

$$u_y(z) = \frac{1}{2\mu}\frac{p_1 - p_2}{L}\left[\left(\left(\frac{\delta}{2}\right)^2 - z^2\right)\right] \tag{4.27}$$

$$\vec{\mathrm{u}} = \frac{1}{a\delta}\int_{-\frac{\delta}{2}}^{\frac{\delta}{2}}\int_{0}^{\mathrm{a}} u_y(z)dydz \tag{4.28}$$

$$\vec{\mathrm{u}} = \frac{1}{2\mu\delta}\frac{p_1 - p_2}{L}\int_{-\frac{\delta}{2}}^{\frac{\delta}{2}}(\left(\frac{\delta}{2}\right)^2 - z^2)dz \tag{4.29}$$

Therefore, average fracture velocity can be written as:

$$u = \frac{\delta^2}{12\mu}\frac{p_1 - p_2}{L} \tag{4.30}$$

Also fracture flow rate is:

$$Q_f = \frac{a\delta^3}{12\mu}\frac{p_1 - p_2}{L} \tag{4.31}$$

It's known that Darcy's flow equation is:

$$\frac{Q}{A} = -\frac{k}{\mu}\frac{\Delta P}{\Delta L} \tag{4.32}$$

Hence, fracture permeability is written as:

$$k_f = \frac{\delta^2}{12} \tag{4.33}$$

It must be noted that equation 4.33 is computed for fracture permeability (k_f) where Darcy's law is applicable (Witherspoon et al., 1979).

4.2 Partial Differential Equations (PDEs) for DFM on COMSOL

COMSOL Multiphysics, is easy to use and provides all physical modules (heat transfer, fluid mechanics, structural mechanics, etc.) in the same program. The Multiphysics program uses the finite element method (FEM) as a numerical solution. FEM is a numerical solution technique which is used to solve various challenging engineering and physical problems. FEM requires careful attention to mesh generation, element discretization, mathematical approximations, the derivation of equations from physics, the consideration of boundary conditions, and validation.
General form of PDE as followed:

$$\frac{\partial(\rho\phi)}{\partial t} + \nabla(\rho \mathrm{u}) = q \tag{4.34}$$

ϕ is porosity, u is the velocity of the fluid, q is the source or sink term.
Where,

$$\mathrm{u} = \left(-\frac{k}{\mu}\right)\nabla p \tag{4.35}$$

4.3 Partial Differential Equations (PDEs) for MINC on COMSOL

General form of PDE as followed:

$$e_a \frac{\partial^2 p_i}{\partial t^2} + d_a \frac{\partial p_i}{\partial t} + \nabla \cdot (-c\nabla p_i - \alpha p_i + \gamma) + \beta \cdot \nabla p_i + a p_i = f_i \qquad (4.36)$$

$$\nabla = \left[\frac{\partial}{\partial x}, \frac{\partial}{\partial y}\right] \qquad \text{in 2D} \qquad (4.37)$$

e_a is mass coefficient term, d_a is damping, a is absorption coefficient, c is the diffusion coefficient, α conservative flux convection coefficient in x&y direction, β convection coefficient in x&y direction, γ conservative flux source in x& y direction. f_i is the source term (*e_a, a,* β, α, γ are neglegted*)*.

The diffusion coefficient of the rock matrix and homogenous for matrix-to-matrix flow, however, it must be considered for the flow from the 1st matrix (second volume element) to the fracture (the first volume element).

Hence PDE becomes:

$$d_a \frac{\partial p_i}{\partial t} + \nabla(-c\nabla \mathrm{p}_i) = f_i \qquad (4.38)$$

The first term of the equation 4.38, the rate of change of fluid mass within the porous medium with respect to time (or in other words accumulation), is modified as follows:

$$\rho = \frac{pM}{RT} \qquad (4.39)$$

$$\frac{\partial \rho}{\partial t} = \frac{M}{RT} \frac{\partial \mathrm{p}}{\partial t} \qquad (4.40)$$

The damping terms approximately equals:

$$d_a = \phi \frac{M}{RT} \tag{4.41}$$

Change in porosity with time is neglected.

The first term of the equation 4.38 is derived:

$$d_a \frac{\partial \rho_i}{\partial t} = \frac{\partial (\rho \phi)}{\partial t} \tag{4.42}$$

The second term of equation 4.38, the convective flow of fluid within the porous medium, can be written as:

$$\nabla(-c\nabla \mathrm{p}) = \nabla\left(-\rho_i\left(-\frac{k}{\mu}\right)\nabla p\right) \tag{4.43}$$

Where,

$$c = \rho\left(-\frac{k}{\mu}\right) \tag{4.44}$$

$$\nabla(-c\nabla \mathrm{p}) = \nabla(-\rho \mathrm{u})) \tag{4.45}$$

Now, inserting eqn. 4.42 and eqn. 4.45 into the eqn. 4.38*:*

$$\frac{\partial (\rho \phi)}{\partial t} + \nabla(\rho \mathrm{u}) = f_{\mathrm{i}} \tag{4.46}$$

For the source or sink term (f_i) calculation,

$$f_i = \frac{-(q_{i,i+1}\rho_i)}{V_{n,i} f_{\mathrm{i}}} \qquad i = 1 \tag{4.47}$$

$$f_i = -\left(\frac{q_{i,i+1}\rho_i}{V_{n,i}f_i}\right) + \left(\frac{q_{i-1,i}\rho_{i-1}}{V_{n,i}f_i}\right) \qquad i = 2 \ldots \ldots N-1 \tag{4.48}$$

$$f_i = \left(\frac{q_{i-1,i}\rho_{i-1}}{V_{n,i}f_i}\right) \qquad i = N \tag{4.49}$$

Where N is the number of nested blocks.
COMSOL Multiphysics utilizes these equations to solve MINC models numerically.

4.4 Nested Volume Elements

Some parameters are required in order to design MINC model. First, it's important to mention that each nested element has a certain volume fraction (noted as f_j). Volume fraction is the ratio of one nested element to total volume of nested elements. Therefore, volume fraction summation is equal to 1 in all circumstances. Besides volume fractions, distances, interface areas, porosity permeability and exchange (transmissibility) parameters are defined for each nested element. There are a couple of methods to calculate each parameter correctly.

- Equal Volume MINC Method:

Each nested block has the same volume fractions in this method. Interface areas and the distances between the nested elements are calculated from the constant volume fractions.

- Equal Distance MINC Method:

All the distance between each nested element is equal to each other. Other parameters are calculated based on this geometry.

- Logarithmically Distanced MINC Method:

Nested blocks are distanced logarithmically from the fracture.

- Exponentially Distanced MINC Method:

Nested elements are spaced natural logarithmically away from the fracture.

- Commercial-simulator-default MINC Method:

This approach uses CMG (Computer Group Modelling Ltd.) default volume fractions to decide the geometric distance and interface areas between the nested elements.

4.5 MINC Parameter Determination

Three sets of infinite fracture plane, fracture aperture, and spacing (one side length of idealized matrix cube) are idealized in Figure 2.1 MINC model assumes that fracture planes are parallel to matrix blocks. Fracture is the outermost element in Figure 4.4, shown by the dashed line; the inners represent matrix elements. Arranging the distances of each matrix block from the fracture requires consideration of the thermodynamics of each block, as discussed in the mass conservation partial differential equations of the MINC model.

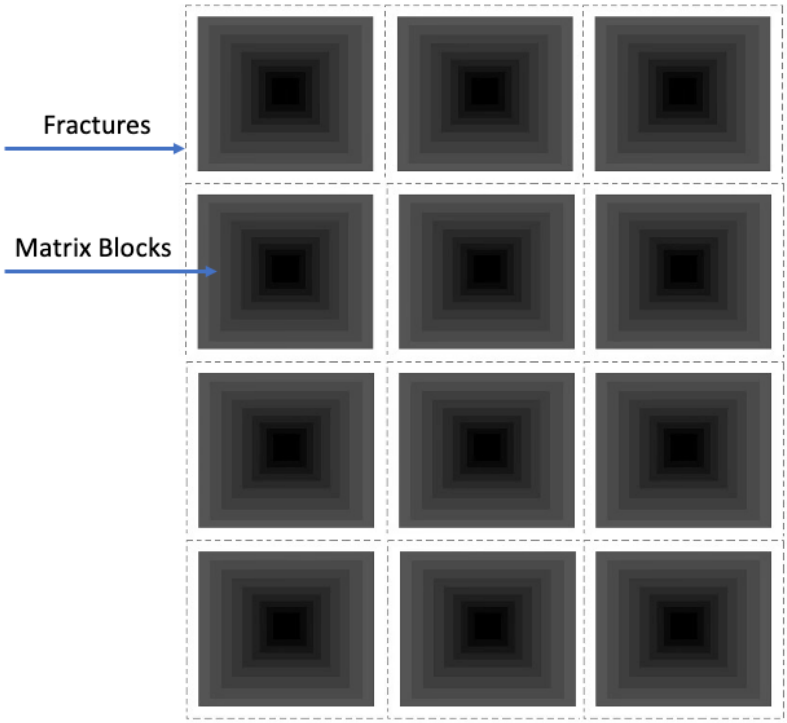

Figure 4.4 Basic computational mesh for fractured porous media

Geometry parameters ($d_{i,j}$ nodal distances, $A_{i,j}$ interface areas, V_j element volumes) for the nested blocks are obtained from a specification of the volume fraction, f_j (Pruess & Narasimhan, 1985). The outermost element is the fracture continuum where j=1.

Equations from 4.50a to 4.56a, which describe idealized matrix cubes nested one by one in Figure 2.1, were adapted from Pruess & Narasimhan(1985). Additionally, 2D versions of these equations, represented as equations from 4.50b to 4.56b for identical squares in Figure 4.4, are derived.

$$f_1 = [L^3 - (L - \delta)^3]/L^3 \approx 3\delta/\mathrm{L} \qquad (4.50a)$$

$$f_1 = \frac{L^2 - (L - \delta)^2}{L^2} = \frac{2\mathrm{L}\delta - \delta^2}{\mathrm{L}^2}$$

$$f_1 = [L^2 - (L - \delta)^2]/L^2 \approx 2\delta/\mathrm{L} \quad (4.50b)$$

$$V_j = f_j L^3 \quad (j = 1 \ldots J) \quad (4.51a)$$

$$V_j = f_j L^2 \cdot 1[m] \quad (j = 1 \ldots J) \quad (4.51b)$$

L^2 is multiplied by 1[m] to arrange volume (V_j) unit for 2D problem.

$$A_{j,j+1} = 6L^3 \left(\sum_{i=j+1}^{J} f_i\right)^{\frac{2}{3}} \quad (j = 1 \ldots J - 1) \quad (4.50a)$$

$$A_{j,j+1} = 4L \left(\sum_{i=j+1}^{J} f_i\right)^{\frac{1}{2}} \cdot 1[m] \quad (j = 1 \ldots J - 1) \quad (4.52b)$$

$A_{j,j+1}$ is multiplied by 1[m] to arrange area unit (m^2) for 2D problem.

Nodes are located at the middle point of inner and outer element surfaces except the 1st one locating where the 2nd nested block starts (see Figure 5.12). The number of nested blocks (N) equals to the number of nodes. Nodal distance means the distance between two nodes (i.e., $d_{1,2}$ is the distance between node 1 and node 2).

$$d_{1,2} = \frac{L}{4}\left[\left(\sum_{i=2}^{J} f_i\right)^{\frac{1}{3}} - \left(\sum_{i=3}^{J} f_i\right)^{\frac{1}{3}}\right] \quad (4.53a)$$

$$d_{1,2} = \frac{L}{4}\left[\left(\sum_{i=2}^{J} f_i\right)^{\frac{1}{2}} - \left(\sum_{i=3}^{J} f_i\right)^{\frac{1}{2}}\right] \quad (4.53b)$$

$d_{1,2}$, the distance locates from the beginning of the 2nd nested block to the middle point of the 2nd (1st matrix block) and 3rd (2nd matrix block) nested elements. $d_{1,2}$ is shown in Figure 5.12 physically.

$$d_{j,j+1} = \frac{L}{4}[(\sum_{i=j}^{J} f_i)^{\frac{1}{3}} - (\sum_{i=j+2}^{J} f_i)^{\frac{1}{3}}] \ \ldots (j = 2 \quad J-2) \tag{4.51a}$$

$$d_{j,j+1} = \frac{L}{4}[(\sum_{i=j}^{J} f_i)^{\frac{1}{2}} - (\sum_{i=j+2}^{J} f_i)^{\frac{1}{2}}] \ \ldots (j = 2 \quad J-2) \tag{4.52b}$$

$d_{j,j+1}$ is the distance between j^{th} and $j+1^{th}$ nodes and from $d_{2,3}$ to $d_{j-2,j-1}$ is calculated by the equation 4.54.

$$d_{J-1,J} = \frac{L}{4}(f_{J-1} + f_J)^{\frac{1}{3}} - \frac{3L}{20} f_J^{\frac{1}{3}} \tag{4.53a}$$

$$d_{J-1,J} = \frac{L}{4}(f_{J-1} + f_J)^{\frac{1}{2}} - \frac{L}{8} f_J^{\frac{1}{2}} \tag{4.55b}$$

The last equation states that the last node, (j=N), is not located in the middle of the innermost element. Instead, it is expected to be positioned near the beginning of the last nested block and explained in detail in Section 4.6. When the variation of thermodynamics properties, such as temperature or pressure around the fracture is small, subdividing volume elements to nested blocks is not required for a cube in Figure 4.4. In other words, thermodynamics are almost the same for the neighboring nested elements so they can be lumped together into one element volume. Therefore, corresponding nested volumes can be merged into one computational volume element. Hence, upscaling of such kind of case, scaling law, is needed when spatial resolution is required for small grids (Vn < < L3) (Pruess & Narasimhan, 1985).
So, the number of elementary units is identified as follows:

$$\sigma = \frac{V_n}{L^3} \tag{4.54a}$$

$$\sigma = \frac{V_n}{L^2 \cdot 1[\,\mathrm{m}]} \tag{4.56b}$$

V_n is the total volume of the elementary unit and σ is an integer number.
So that the volume of continuum j within V_n is:

$$V_{nj} = \sigma V_j = f_j V_n \tag{4.57}$$

Therefore, interface area occurs σ times so that:

$$A_{nj,nj+1} = \sigma A_{j,j+1} \tag{4.58}$$

And the nodal distances equation does not change since the distances depend only on geometry instead of dimension, so:

$$d_{nj,nj+1} = d_{j,j+1} \tag{4.59}$$

4.6 Validity of 2D MINC Formulas

The calculations for distance, volume, and area in a 2D model are not found in the literature. Firstly, 2D geometry is created to use these formulas. For example, constant volume fraction value for all matrix continua is found by dividing the rest of volume fractions (from fracture fraction) to the nested matrix continua number for equal volume method. For another example, the relationship between the distances is established for each distance method (i.e., equal, exponentially, logarithmically distanced) and then their volume fractions are completed based on geometry. After deciding volume fractions from both examples, equations from 4.53b to 4.55b are created to match these formulas with the distances already created geometrically. In

addition, to validate these formulas (eqns. from 4.50b to 4.56b), MATLAB code, based on proximity function, is created, and attached to appendices.

4.6.1 Proximity Function

Proximity function explains matrix fracture interaction based on the geometry of the nested blocks. In fact, points are distributed in a line randomly and then, Monte Carlo integration techniques are applied to compute nodal distances ($d_{i,j}$) for irregular shape matrix or proximity functions are derived analytically to compute distances for regular shaped matrix blocks. This function calculates the volume of each matrix continuum as a function of the distance (x_i in Figure 4.8) from the fracture (Pruess & Karasaki, 1982).

Volume fractions are the only necessary parameters to compute all geometry by proximity function to understand interporosity flow between matrix and fractures (Farah et al., 2016).

Proximity function P(x) is used, firstly, to calculate volume fraction of matrix blocks from fracture volume fraction:

$$V_m = (1 - f_1)V_0 \tag{4.55}$$

V_0 is the total volume of the volume element, V_m is the total matrix volume, f_l is the fracture volume fraction.
V(x) is volume of the matrix which is distanced x from the fracture faces (see Figure 4.8). V(x) is written as a function of P(x):

$$V(x) = P(x)V_m \tag{4.56}$$

4.6.1.1 Proximity function for 1D:

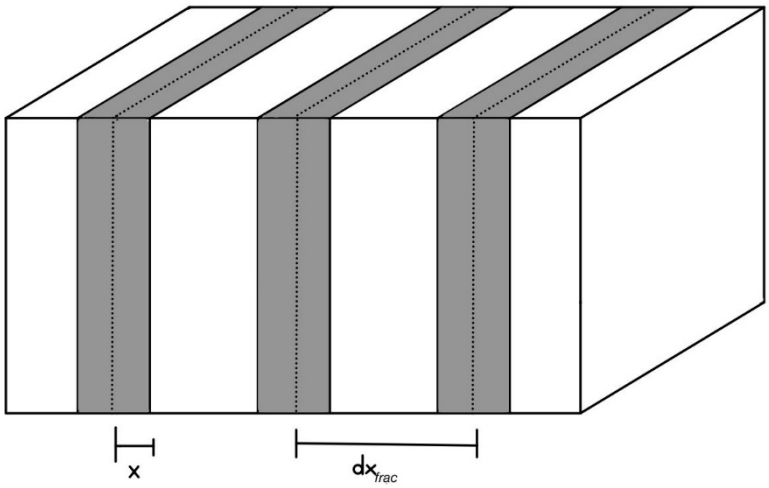

Figure 4.5 1D fracture system

Proximity function for 1D fracture system is given by:

$$u = 2 \cdot \frac{x}{dx_{frac}} \tag{4.62}$$

$$P(x) = \begin{cases} u, & 2x < dx_{frac} \\ 1, & 2x \geq dx_{frac} \end{cases} \tag{4.63}$$

Where x is the half of fracture aperture, $d_{x_{frac}}$ is the fracture spacing (or length of one elementary unit).

4.6.1.2 Proximity function for 2D:

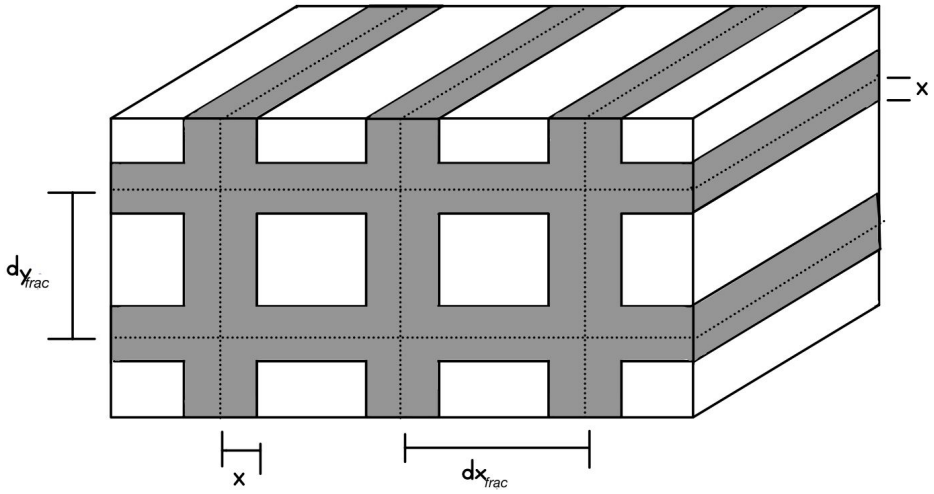

Figure 4.6 2D fracture system

Proximity function for 2D fracture system is given by:

$$u = 2 \cdot \frac{x}{dx_{frac}} \tag{4.64}$$

$$v = 2 \cdot \frac{x}{dy_{frac}} \tag{4.65}$$

$$P(x) = \begin{cases} u + v - uv, & 2x < \min\left(dx_{frac}, dy_{frac}\right) \\ 1, & 2x \geq \min\left(dx_{frac}, dy_{frac}\right) \end{cases} \tag{4.66}$$

4.6.1.3 Proximity function for 3D:

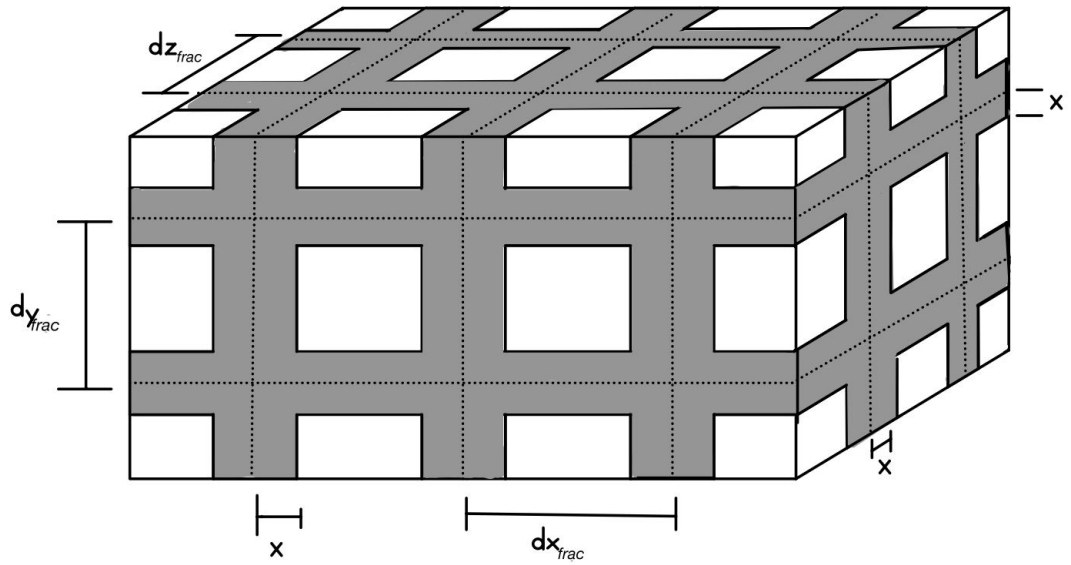

Figure 4.7 3D fracture system

Proximity function for 3D fracture system is given by:

$$u = 2 \cdot \frac{x}{dx_{frac}} \tag{4.67}$$

$$v = 2 \cdot \frac{x}{dy_{frac}} \tag{4.68}$$

$$w = 2 \cdot \frac{x}{dz_{frac}} \tag{4.69}$$

$$P(x) = \begin{cases} u + v + w - uv - vw - uw + uvw, & 2x < \min(dx_{frac}, dy_{frac}, dz_{frac}) \\ 1, & 2x \geq \min(dx_{frac}, dy_{frac}, dz_{frac}) \end{cases}$$

(4.57)

Secondary mesh is created by using fracture volume fraction and proximity function by primary mesh. Proximity function P(x) is used, secondly, to calculate the distances between nested blocks and interface areas between the elements.

As mentioned before, each element is divided into N-nested elements. Flow occurs only in fractures (DP model is assumed). To understand flow behavior between two neighbors (i.e., x_i and x_{i+1} in Figure 4.8) continua, x_i calculation based on proximity function is required.

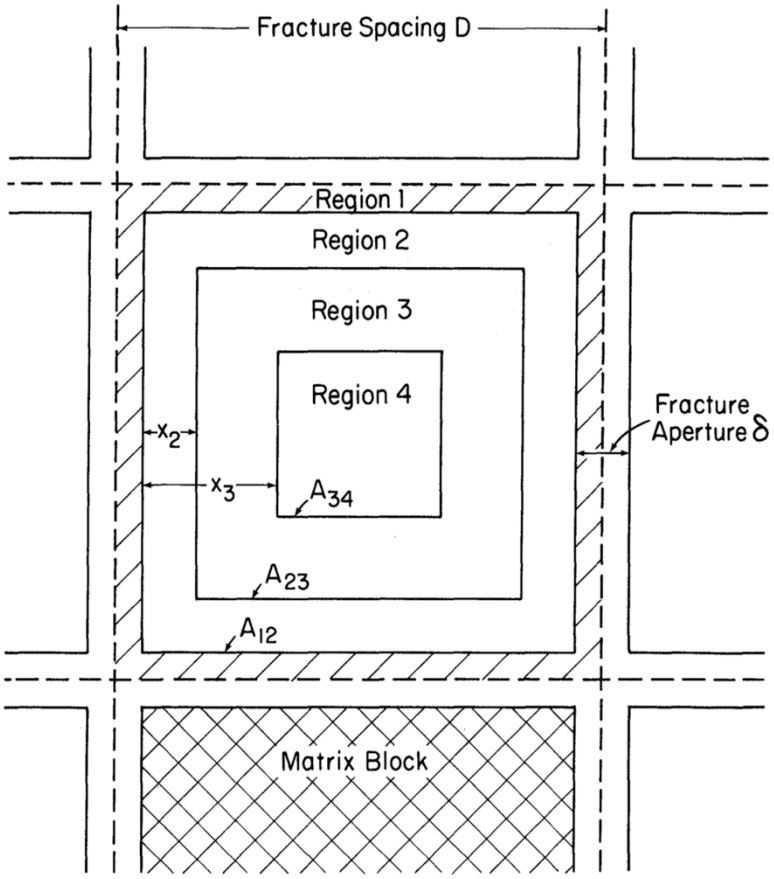

Figure 4.8 MINC partitioning of an idealized fracture system (Pruess, 1983)

The volume fractions of the nested rock matrix elements f_i for $2 \leq i \leq N$

Thanks to the definition of proximity function, $P(x_i)$ for any nested element can be written as:

$$P(x_i) = \frac{V(x_i)}{V_m} \qquad \text{for i} > 1 \tag{4.71}$$

The interface area at a distance x (from fracture) is derived from the equation 4.71 and 4.60:

$$A(x) = \frac{dV}{dx} = (1 - f_1)V_0 \frac{dp(x_i)}{dx} \tag{4.72}$$

Using the volume fractions eqn. 4.71 becomes:

$$P(x_i) = \frac{\sum_{j=2}^{i} f_i V_0}{(1 - f_i)V_0} \tag{4.73}$$

or

$$P(x_i) = \frac{\sum_{j=2}^{i} f_i}{(1 - f_1)} \tag{4.74}$$

The nodal distances can be written in terms of x_i:

$$d_{1,2} = \frac{x_2}{2} \tag{4.75}$$

$$d_{i,i+1} = \frac{x_{i+1} - x_i}{2} - \frac{x_i - x_{i-1}}{2} \qquad i = 2 \ldots N - 2 \tag{4.76}$$

Equation 4.73 is solved by using bisection method in MATLAB (i.e., x_i value is researched by iteration that provides $P(x_i)$ in the equation 4.73, x_1 is located on the fracture interface so it equals to 0).

To calculate $x_{N,}$, or D_i the innermost nodal distance, different method is applied .

$$d_{i-1,i} = \frac{x_{i-1} - x_{i-2}}{2} + D_i \qquad for\ i = N \tag{4.77}$$

To accurately estimate the pressure gradient at the interface between two of the innermost elements, it is necessary for the last node to be positioned closer to the beginning of the innermost element, rather than at its middle. The determination of this distance, denoted as 'D', is based on finite difference approximation to accurately describe fluid flow between continua. D is a function of time in transient fluid flow regimes, and selecting the optimal D values is crucial for use in quasi-steady state flow regimes (Pruess, 1983).

D can be calculated from the following table:

Table 4.1 Quasi-steady flow distances for rectangular matrix blocks (Warren & Root, 1963)

Case	Dimensions of matrix blocks	Dimensions of innermost blocks	Average linear dimension of innermost block	D_J
1-D	a	$u=a-2x_{J-1}$	$\ell = u$	$\ell/6$
2-D	a	$u=a-2x_{J-1}$	$\ell = \frac{2uv}{u+v}$	$\ell/8$
	b	$v=b-2x_{J-1}$		
3-D	a	$u=a-2x_{J-1}$	$\ell = \frac{3uvw}{uv+vw+uw}$	$\ell/10$
	b	$v=b-2x_{J-1}$		
	c	$w=c-2x_{J-1}$		

D is function of dimension of matrix blocks (fracture spacing- fracture aperture) and innermost blocks.

Once the volume fractions are accomplished, The MATLAB code in appendices enables to complete all MINC parameters and validates the equations from 4.50b to 4.56b.

CHAPTER 5

NUMERICAL MODELING

Creating DFM and MINC models on COMSOL Multiphysics program steps are discussed in detail in this section. Models are based on Bristol Channel, which is a real naturally fractured rock along the southern margin of Bristol Channel coast, United Kingdom. The dimension of the reservoir in Figure 5.1 is 18 [m] x 8 [m]. The major component of the Bristol Channel is limestone with interbedded shales, and the fractures are approximately 30 cm high. The created models on COMSOL are assumed to be like a fractured shale gas reservoir made up of only methane in 2D dimensions. The 18 [m] x 8 [m] dimension unstructured grid ASCII file is then converted to upload COMSOL.

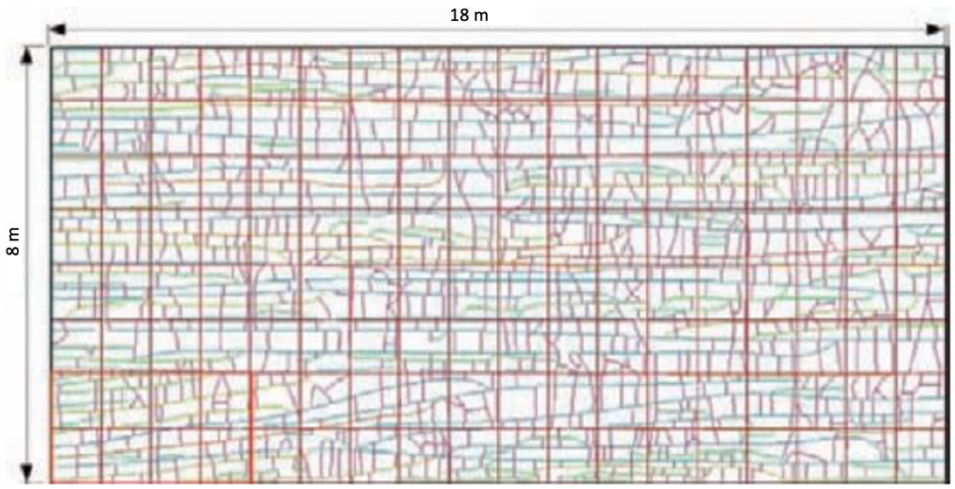

Figure 5.1 Bristol Channel geometry (Tatomir, 2012)

While modeling both DFM and MINC, 4 [m] x 2 [m] section of the Bristol Channel (Figure 5.2) is focused.

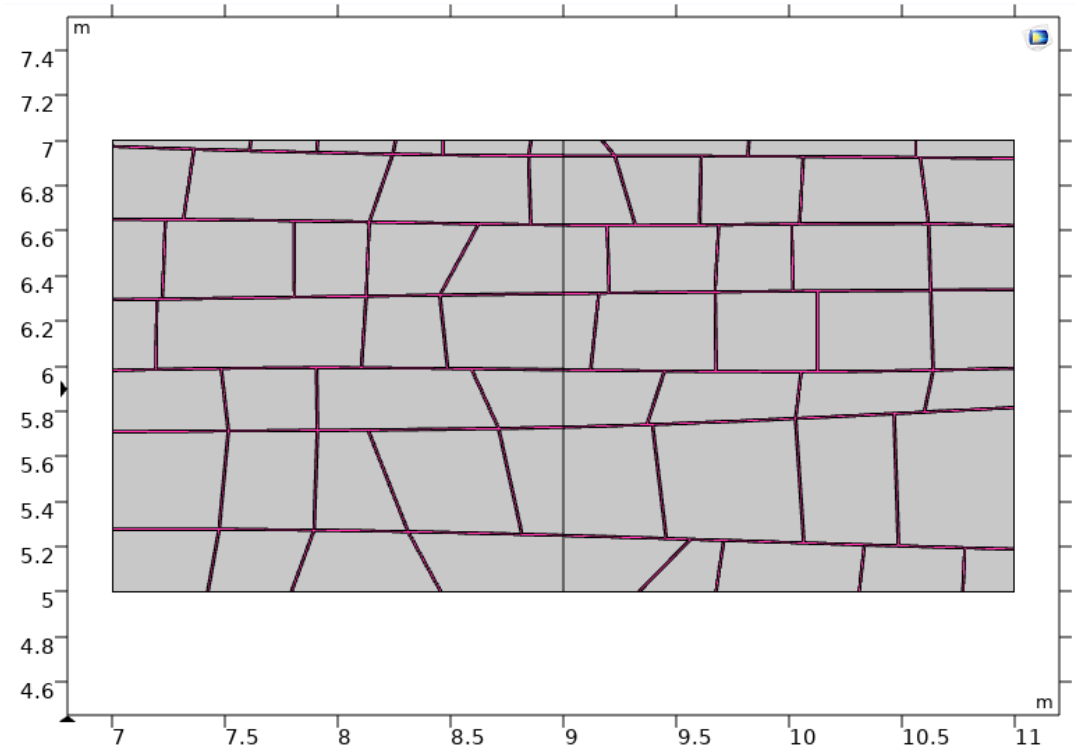

Figure 5.2 Created 4 [m] x 2 [m] dimensions as a representative part of Bristol Channel geometry

Once DFM model is created, five different MINC model approaches are applied and compared with the DFM model. Then, the best representative MINC model is obtained by optimizing volume fractions and matrix permeability.

5.1 DFM Parameters

A certain amount of methane is constantly injected into the fractures (black areas in Figure 5.3) having $1x10^5$ Pa initial reservoir pressure. The model considers the change in properties of methane characteristics. Table 5.1 summarizes the constant source injection problem parameters. Porosity of fracture is taken as 1, and matrix porosity is assumed as 0.18. Darcy's law is applied to the porous media. Matrix permeability is taken as $1x10^{-17}$ m^2 (0.0101 mD) for DFM model. In DFM model, fracture aperture is taken as 0.01 [m], and fracture permeability is calculated by using it.

Table 5.1 DFM Constant Source Injection Problem Parameters

Domain Properties	DFM Parameters
Fracture aperture	0.01m
Matrix permeability	$1x10^{-17}$ m²
Fracture permeability	$8.3333x10^{-6}$ m² (from Equation 4.33)
Matrix porosity	0.18
Fracture porosity	1
Initial Condition	$1x10^{5}$ Pa
Boundary Condition	1/6000 (kg/s) source into fractures shown in Figure 5.3

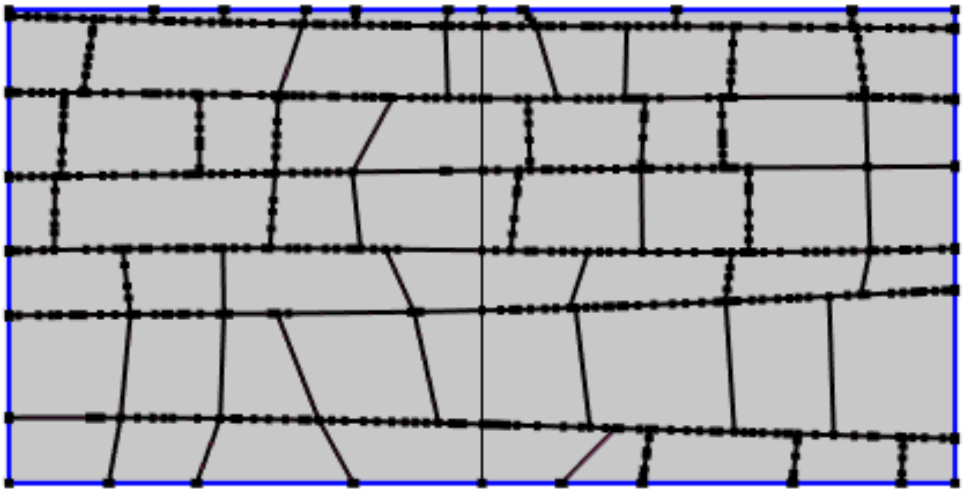

Figure 5.3 Constant source injection problem with no flow boundaries (indicated by blue lines)

5.1.1 Finite Element Grid Creation (Meshing)

COMSOL Multiphysics program creates meshing and the size changes from extremely fine to extremely coarse. COMSOL creates mesh properly as triangle shape for 2D problems and tetrahedral for 3D problems.

Even though normal size mesh is created in DFM, the computation time is enormously high. Discretization is expectedly high around fractures (see Figure 5.4). Hence, the number of triangles increases and the size of them decreases when getting close to fractures. If a finer mesh is used, the program needs higher computational power due to the increased level of discretization.

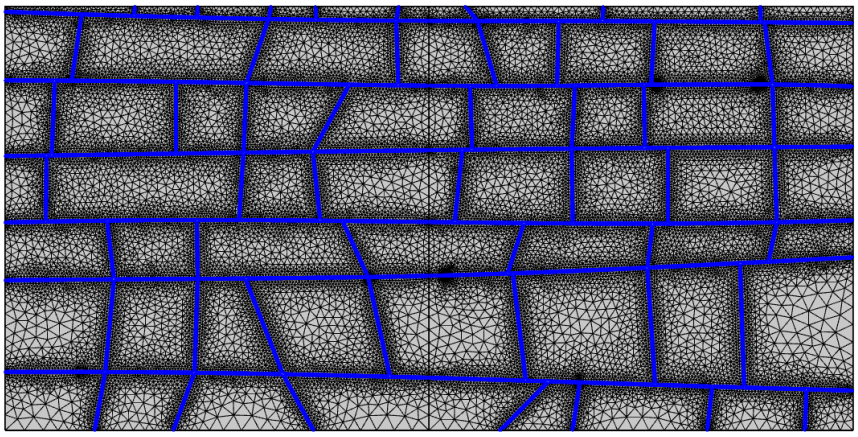

Figure 5.4 DFM model meshing

5.2 MINC Parameters – Upscaling

Upscaling is the process to adjust or transform properties or characteristics from a smaller or more detailed scale to a larger or coarser scale. This is frequently undertaken to enhance the computational efficiency of complex models or to extend their applicability to a wide range of reservoirs. It can entail methods like averaging, simplification, or other adjustments to make characteristics from the DFM model suitable for use in the MINC models. Table 5.3 represents domain properties for MINC models clearly.

5.2.1 Matrix-Fracture Volumes

While creating DFM model on COMSOL, uniform fracture aperture is taken as 0.01[m]. Fracture volume of DFM must be in accordance with the first domain of

MINC model. Therefore, fracture volume fraction (f_l) is based on the volume of fracture in DFM.

5.2.2 Fracture Permeability

DFM model, is created as a constant pressure boundary problem to decide transmissibility in the middle of the domain in Figure 5.6. Flow mainly occurs through interconnected fractures. In Figure 5.6, high pressure and low pressure is arranged on the left and on the right boundaries respectively. Upscaled fracture permeability for MINC models can be computed from the transmissibility equation by (Karimi-Fard et al., 2006) for a steady state problem. Table 5.2 summarizes DFM parameters for this model.

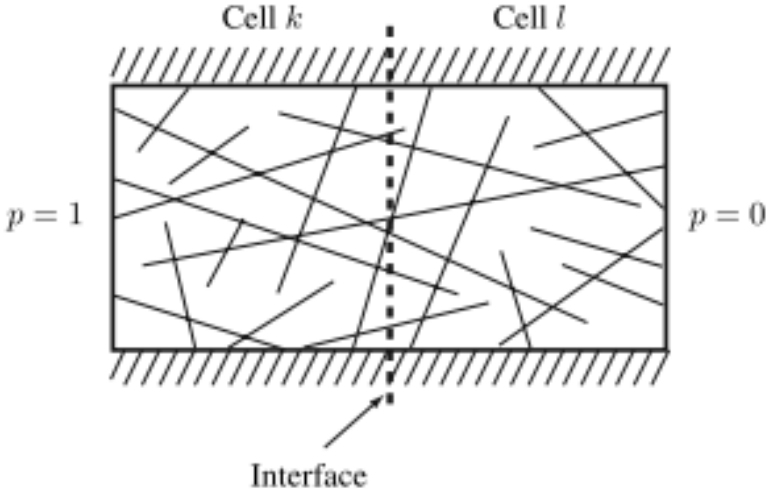

Figure 5.5 Schematic illustrating transmissibility upscaling (Karimi-Fard et al., 2006)

$$\tau^{k,l} = \frac{Q^{k,l}\mu}{\bar{\rho}(\bar{p}^k - \bar{p}^l)} \tag{5.1}$$

$\tau^{k,l}$ is the transmissibility between left and right domain boundary in Figure 5.5.

$Q^{k,l}$ is the flow rate through the interface, $\bar{p}^k$ is the average pressure of cell k, $\bar{p}^l$ is the average pressure of cell l, $\bar{\rho}$ is the average density at the interface.

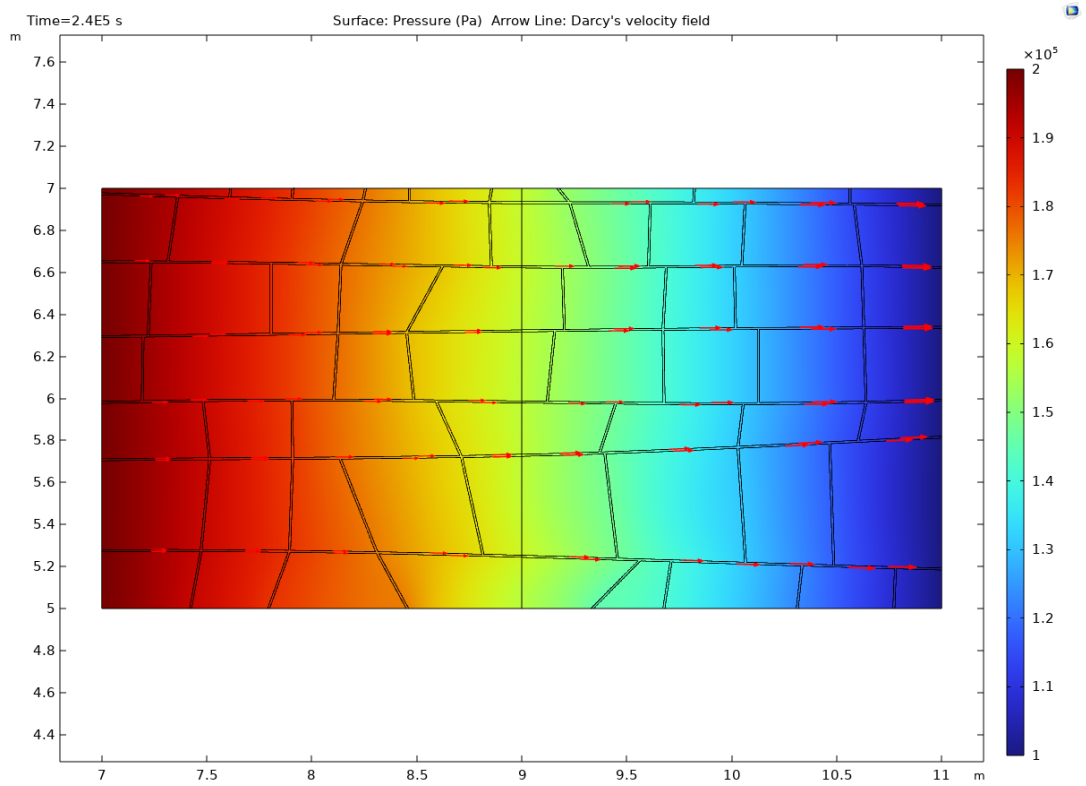

Figure 5.6 Transmissibility upscaling with constant pressure boundary on COMSOL

The left boundary pressure is $2x10^5$ Pa and the right boundary pressure is arranged as $1x10^5$ Pa. Then the model runs for $2.4x10^5$ seconds, where it has already reached to steady state. Fracture permeability for MINC models is calculated as $2.51x10^{-7}$ m^2 when Equation 5.1 is converged.

Table 5.2 DFM Constant Pressure Boundary Problem Parameters

Domain Properties	DFM Parameters
Fracture aperture	0.01 m
Matrix permeability	$1x10^{-17}$ m²
Fracture permeability	$8.3333x10^{-6}$ m²
Matrix porosity	0.18
Fracture porosity	1
Initial Condition	$1x10^{5}$ Pa
Boundary Condition	Left boundary: $2x10^{5}$ Pa
	Right boundary: $1x10^{5}$ Pa

5.2.3 Matrix Permeability

Matrix permeability in MINC models can be roughly calculated from DFM matrix permeability by applying Darcy's Law relationship between the two models as follows:

$$k_{m_{MINC}} \approx k_{m_{DFM}} \cdot \frac{A_{f,m_{DFM}}}{A_{f,m_{MINC}}} \tag{5.2}$$

$k_{m_{MINC}}$ is matrix permeability of MINC model, $k_{m_{DFM}}$ is the matrix permeability of DFM model, $A_{f,m_{MINC}}$ is the total interface area between matrix and fractures in MINC model, $A_{f,m_{DFM}}$ is the total interface area between matrix and fractures in DFM model.

Equation 5.2 gives an approximation result. This value is also optimized according to DFM model result in section 6.3.

Table 5.3 MINC Constant Source Injection Problem Parameters

Domain Properties	MINC Parameters
Fracture aperture	0.0481 (for one volume element)
Matrix permeability	2.79×10^{-16} m² (roughly calculated from Equation 5.2 and optimized later)
Fracture permeability	2.51×10^{-7} m² (upscaled from Equation 5.1)
Matrix porosity	0.18
Fracture porosity	1
Initial Condition	1×10^{5} Pa
Boundary Condition	1/6000 (kg/s) source into fractures with no flow boundary condition same as DFM

5.3 MINC Parameters – Volume Fractions

The most decisive parameter is fracture fraction or in other words, first domain volume fraction. Fracture volume in DFM model must be equal to fracture volume in MINC models. Then, fracture volume fraction is decided with fracture aperture for the first MINC volume. To enhance accuracy, all MINC models are constructed with 10 (N=10) nested elements since greater accuracy is achieved with higher discretization. Figure 5.7 shows the representation of MINC model where each element has 10 nested domains.

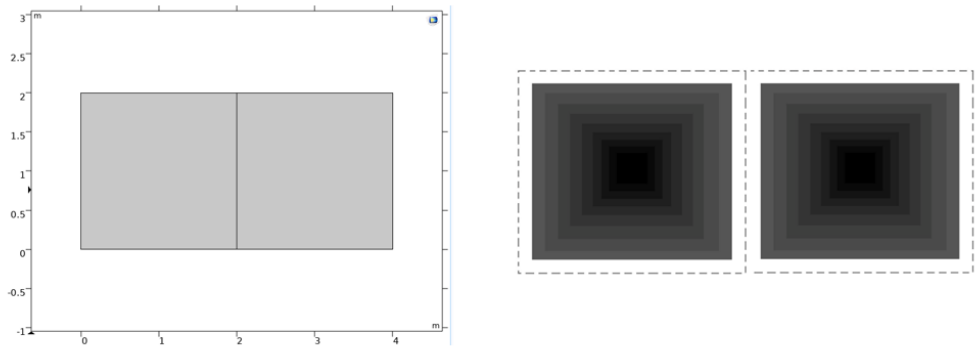

Figure 5.7 Primary Mesh for a MINC model on COMSOL & Computation of nested MINC domains for N=10

To decide each MINC parameters, construction of geometry of each method is required. Table 5.4 summarizes all volume fractions for each method.

Table 5.4 Volume Fractions for five different methods (N=10)

Volume Fractions	Equal volume MINC	Equal Distance MINC Method	Logarithmically Distance MINC (LOG-MINC)	Exponentially Distanced (LN-MINC)	Commercial-simulator-default (SIMD-MINC)
f_1	0.0475	0.0475	0.0475	0.0475	0.0320
f_2	0.1058	0.2109	0.0894	0.1402	0.0580
f_3	0.1058	0.1846	0.0997	0.1437	0.0750
f_4	0.1058	0.1582	0.1022	0.1366	0.0890
f_5	0.1058	0.1318	0.1137	0.1356	0.1010
f_6	0.1058	0.1054	0.1186	0.1242	0.1110
f_7	0.1058	0.0791	0.1304	0.1139	0.1210
f_8	0.1058	0.0527	0.1341	0.0909	0.1300
f_9	0.1058	0.0264	0.1263	0.0581	0.1380
f_{10}	0.1058	0.0033	0.0379	0.0092	0.1450

5.3.1 Equal Volume MINC – Meshing

Volume fraction of fracture is determined by the fracture volume in DFM model. f_l is subtracted from 1 and then divided to 9. The result gives the matrix volume fraction for each nine nested domains. All other geometric parameters are calculated by using equations from 4.51b to 4.55b.

It must be noted that the equation 4.56, σ, number of elementary units within V_n is 1 for all cases. It can be assumed that fractures are distributed around the porous media homogenously. There are two uniform square elementary units where spatial resolution for models is not required.

Computational meshing of equal volume MINC model is in Figure 5.8.

Figure 5.8 Computational meshing of equal volume MINC model

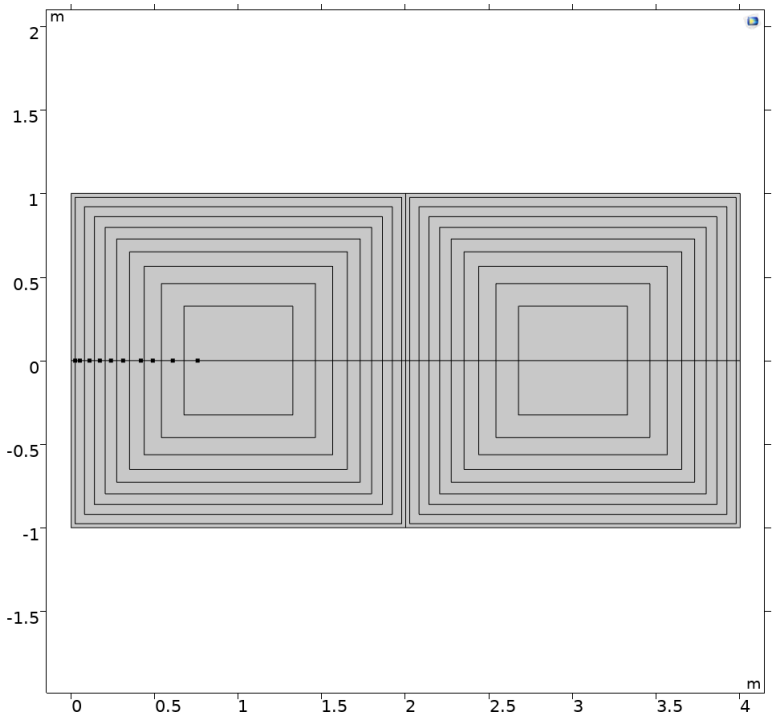

Figure 5.8 Computational meshing of equal volume MINC model

5.3.2 Equal Distance MINC Method – Meshing

In this method, as its name states, nested elements are equally distanced. All distances are assumed equal to each other except for d_{12}. Its length must be equal to the half of each distance due to its geometric location.

Computational meshing of equal distance MINC model is in Figure 5.9.

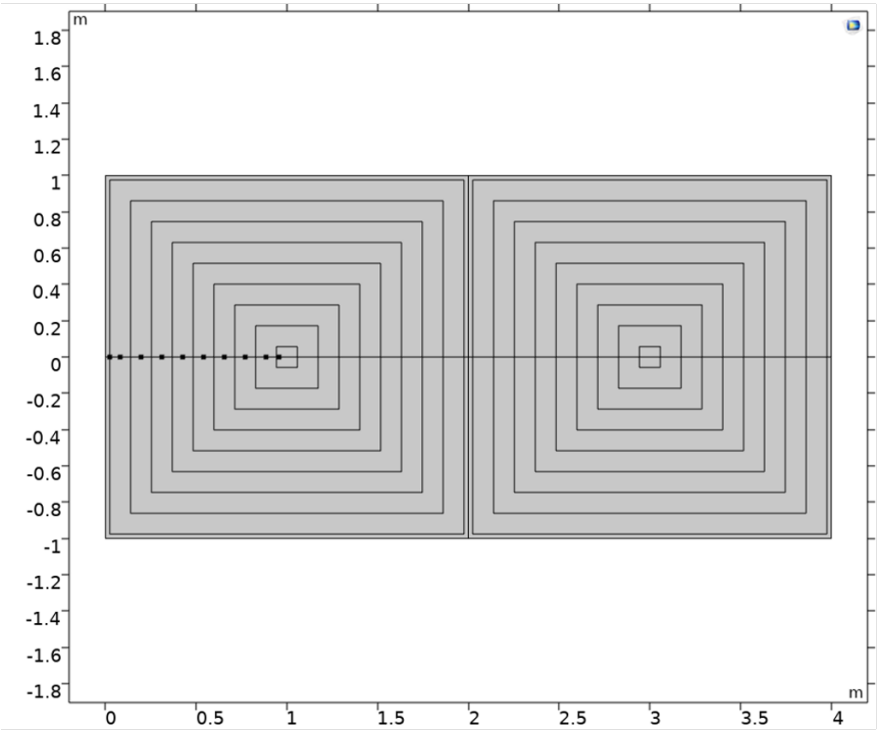

Figure 5.9 Computational meshing of equal distance MINC model

5.3.3 Logarithmically Distanced MINC Method – Meshing

It must be noted that detailed resolution is required around the fracture rather than the innermost matrix. Therefore, the distances must be located closer around the fracture instead of around the innermost volume (Pruess & Narasimhan, 1985). As a result, while creating logarithmically and exponentially distanced models, the nodal distances are arranged as increasing form the fracture to the innermost domain.

Computational meshing of logarithmically distanced MINC model is in Figure 5.10.

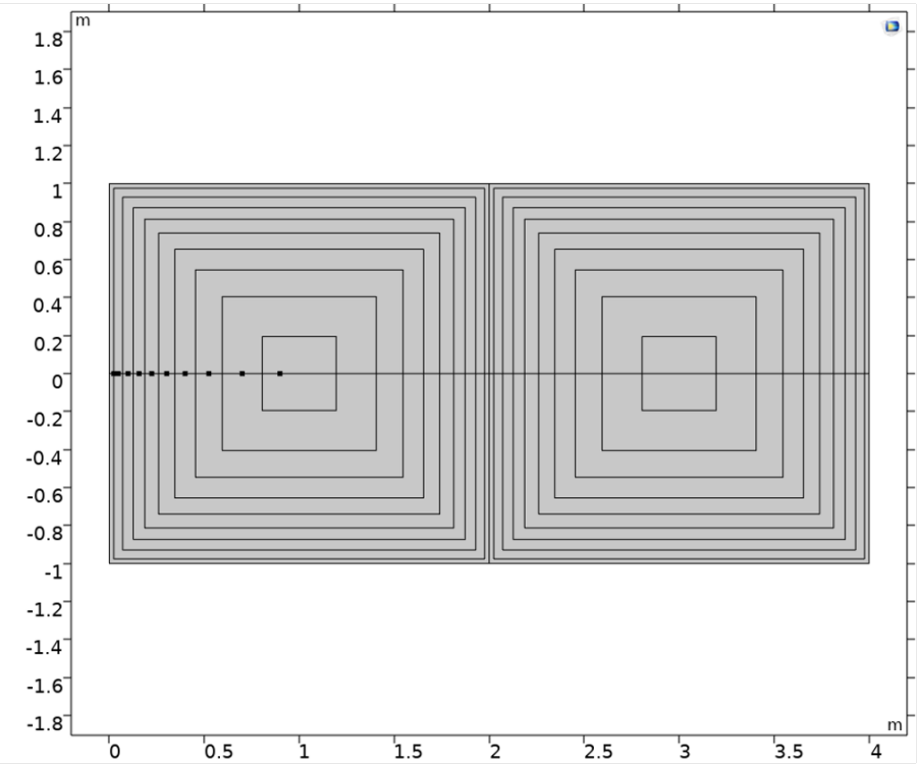

Figure 5.10 Computational meshing of logarithmic distance MINC model

5.3.4 Exponentially Distanced MINC Method – Meshing

Like logarithmically distanced model, the distances are increased from fracture to the middle of the elementary unit.

Computational meshing of exponentially distanced MINC model is shown in Figure 5.11.

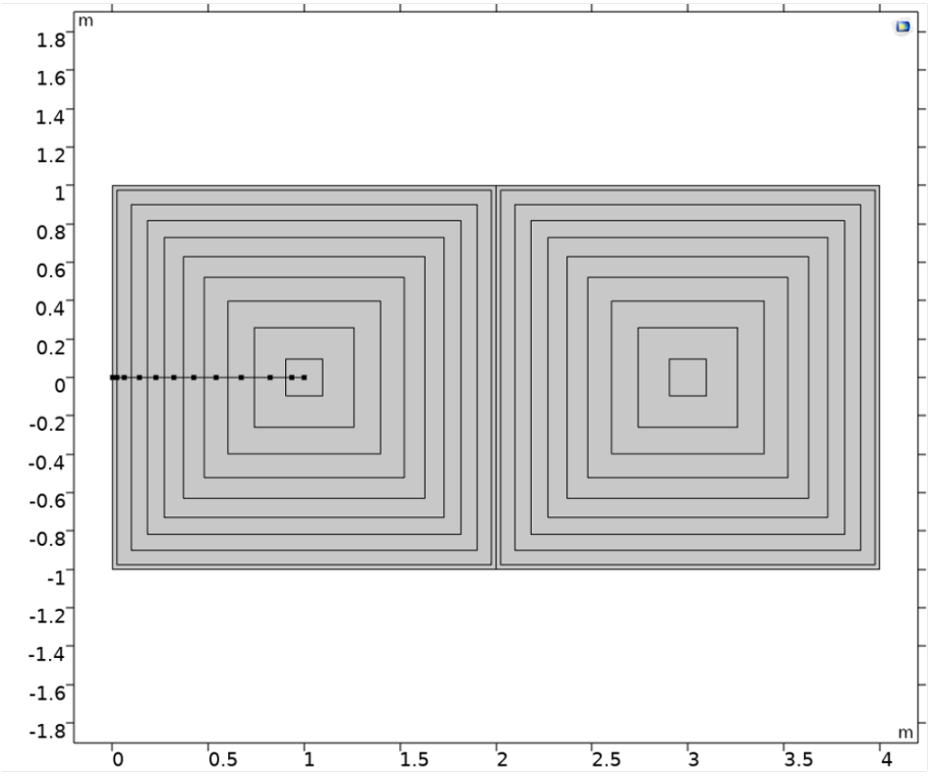

Figure 5.11 Computational meshing of exponentially distanced MINC model

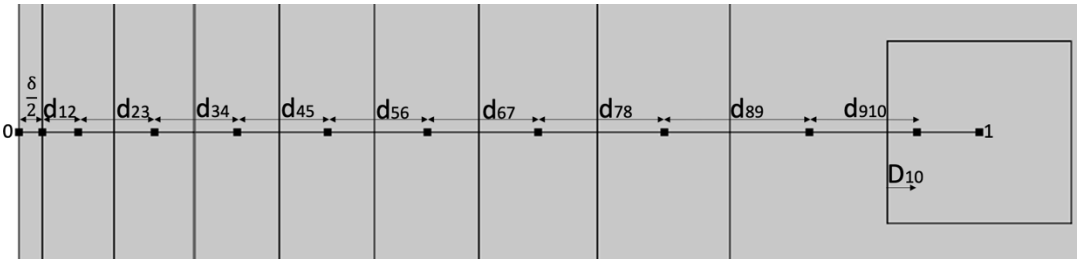

Figure 5.12 Computational meshing of exponentially distanced MINC model - zoomed

The distances between nested elements are shown in Figure 5.12. There are 10 nodes and 9 different nodal distances. (δ is fracture aperture)

5.3.5 Commercial-Simulator-Default (SIMD-MINC) - Meshing

This method is a little bit different than the others. That's because default commercial simulator volume fractions, where CMG is available, are decided to create MINC model (see Table 5.4 for default f_j values).
Computational meshing of Commercial-simulator-default (SIMD-MINC) is in Figure 5.13.

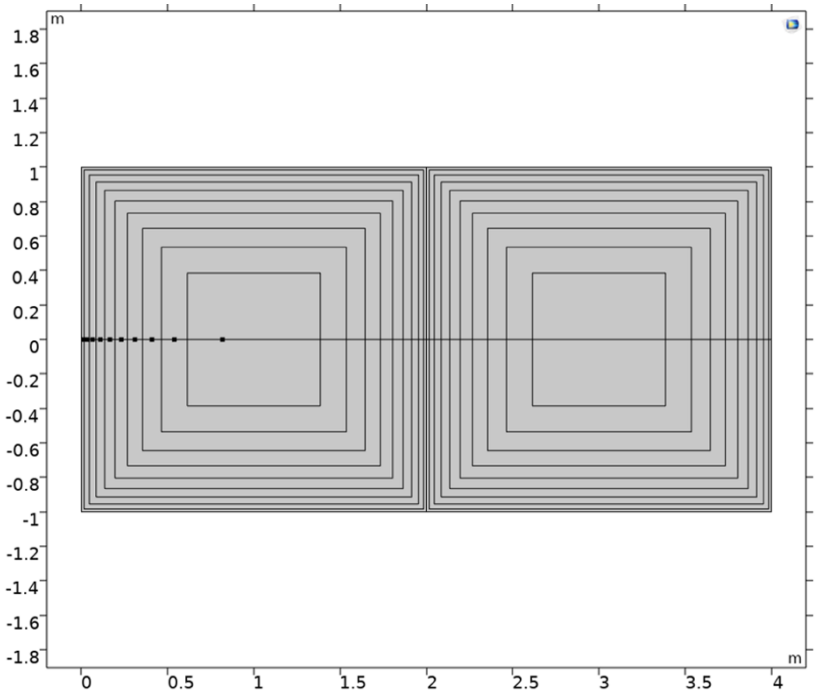

Figure 5.13 Computational meshing of Commercial-simulator-default (SIMD - MINC)

f_l is obviously different than from the other four different methods. Thus, porosity is required to be rearranged both in matrix and fracture, because matrix and fracture volumes of the DFM model should match with MINC model so that this model must be consistent with the other MINC models for comparison purposes.

5.4 Comparison of Model Outputs

Once the models are validated with the initial and boundary condition in Figure 5.3, mass storage vs time graphs are drawn. The same proportion of source is injected to fractures in both models DFM and MINC constantly. The total amount of the accumulated source of DFM is always equal to the source amount of MINC for all methods as it should be (see Figure 5.14) where the total mass storage line of equal volume MINC model exactly matches with the total storage line of DFM model). Figure 5.14 is drawn to check the consistency of the models.

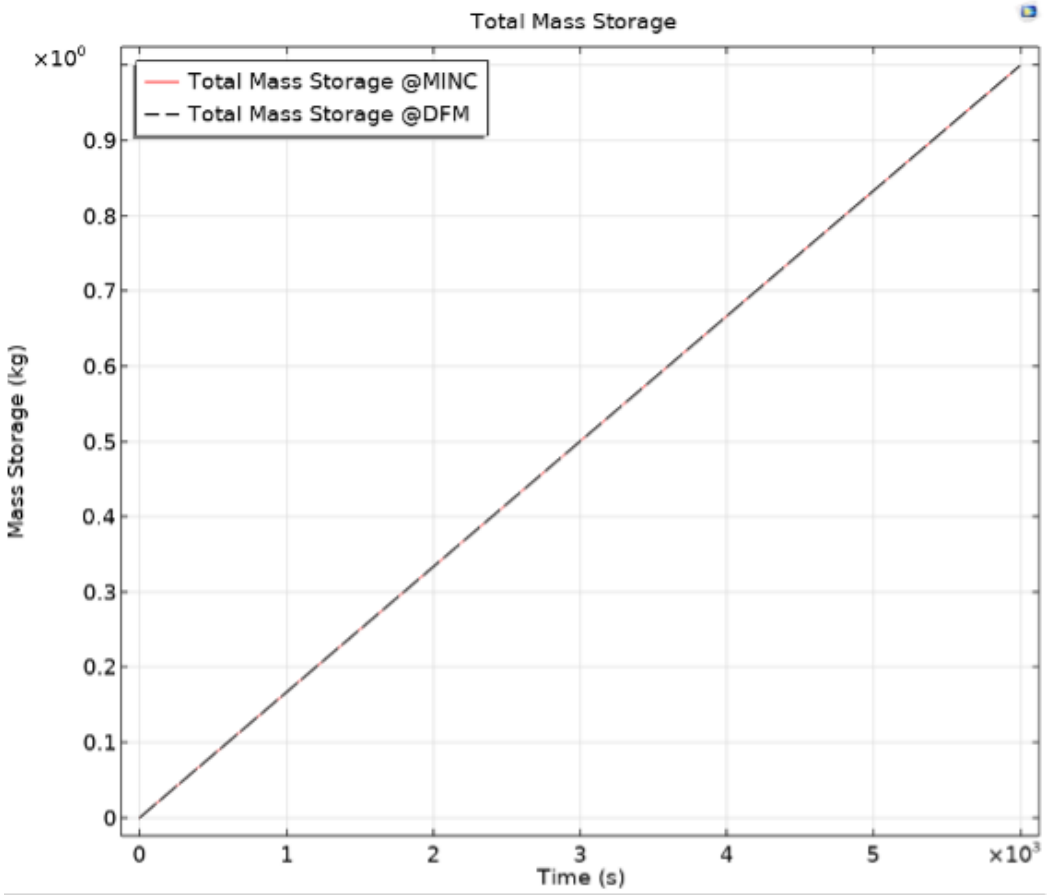

Figure 5.14 Mass storage comparison DFM and MINC model

The accumulated mass in fractures at DFM and at MINC models is expected to give a measure of the accuracy of MINC parameters. The same is valid for the mass in matrix domain for both DFM and MINC models (e.g., Figure 5.15).

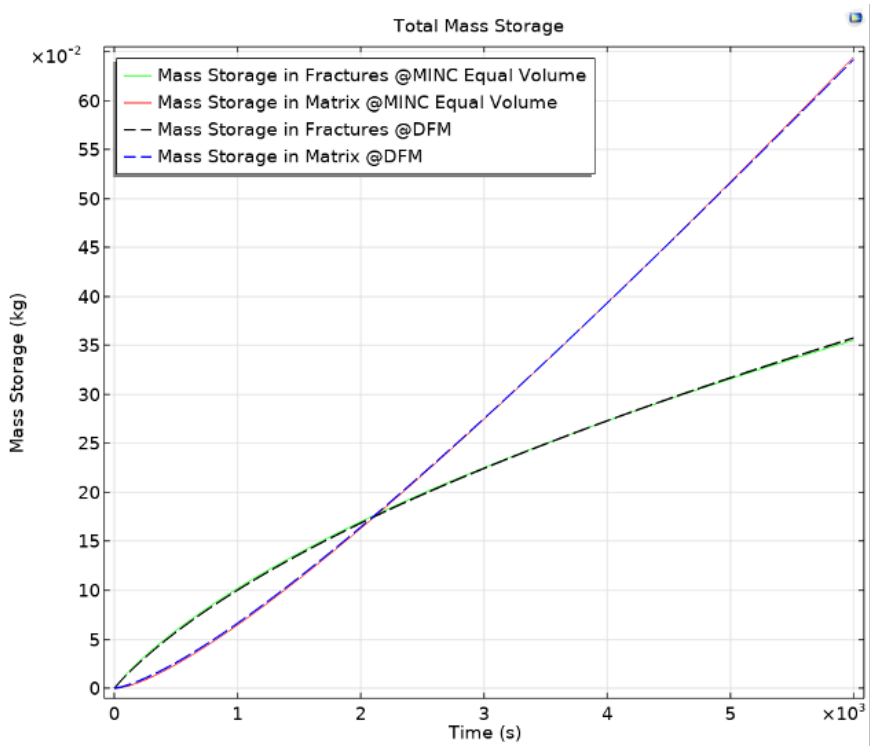

Figure 5.15 Equal volume method comparison with DFM result

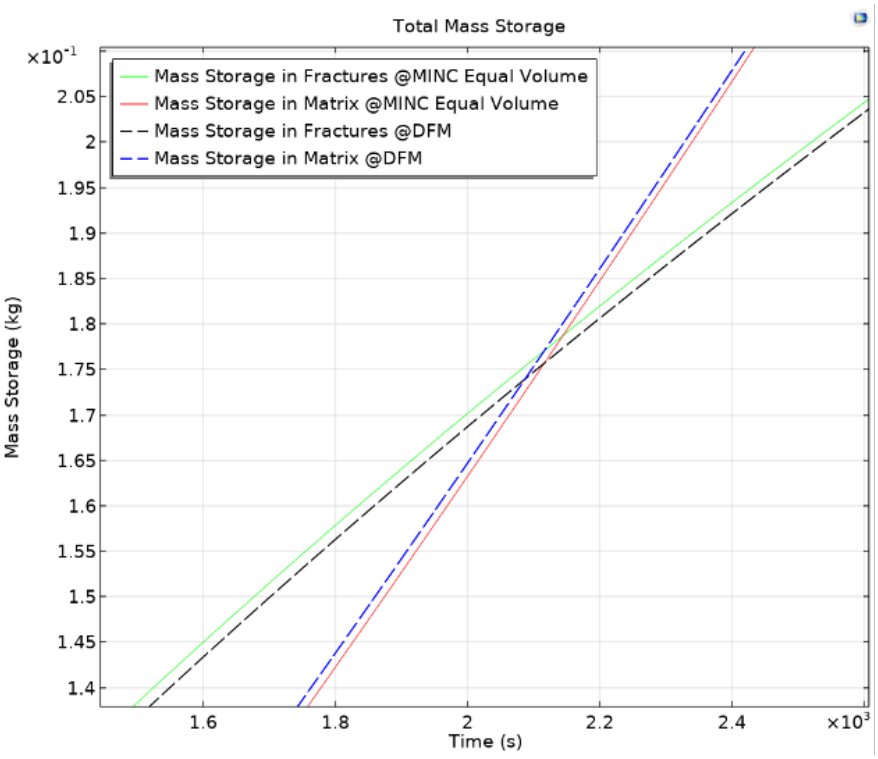

Figure 5.16 Equal volume method comparison with DFM result - zoomed

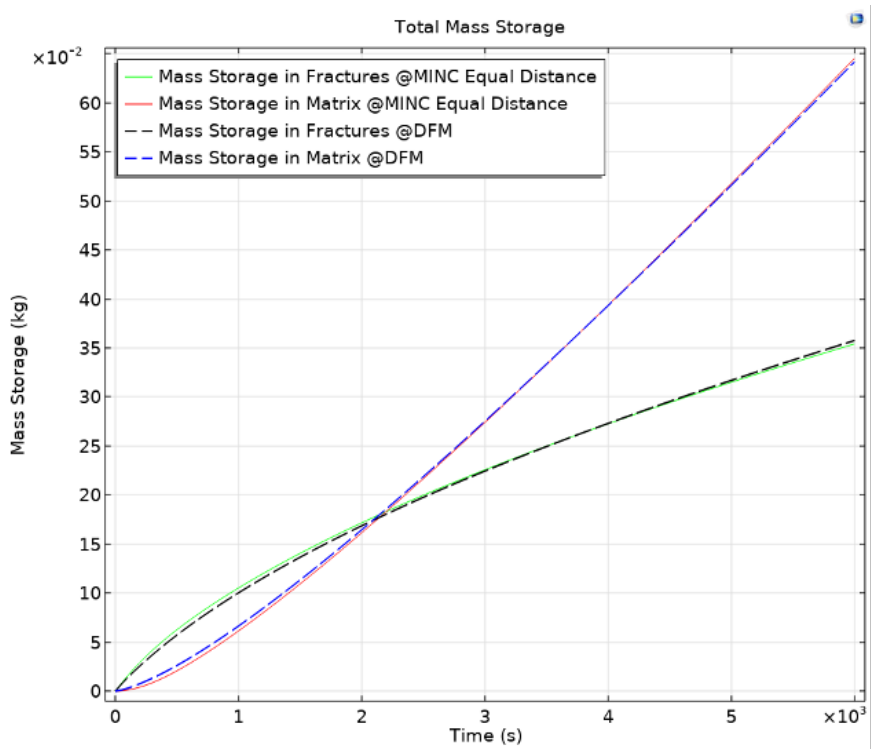

Figure 5.17 Equal distance method comparison with DFM result

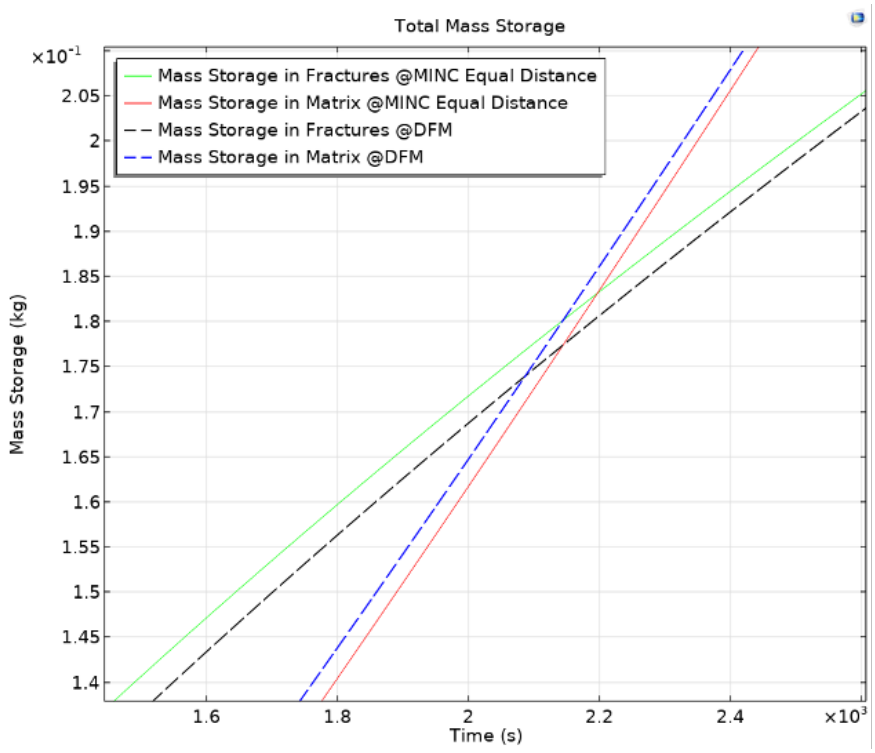

Figure 5.18 Equal distance method comparison with DFM result - zoomed

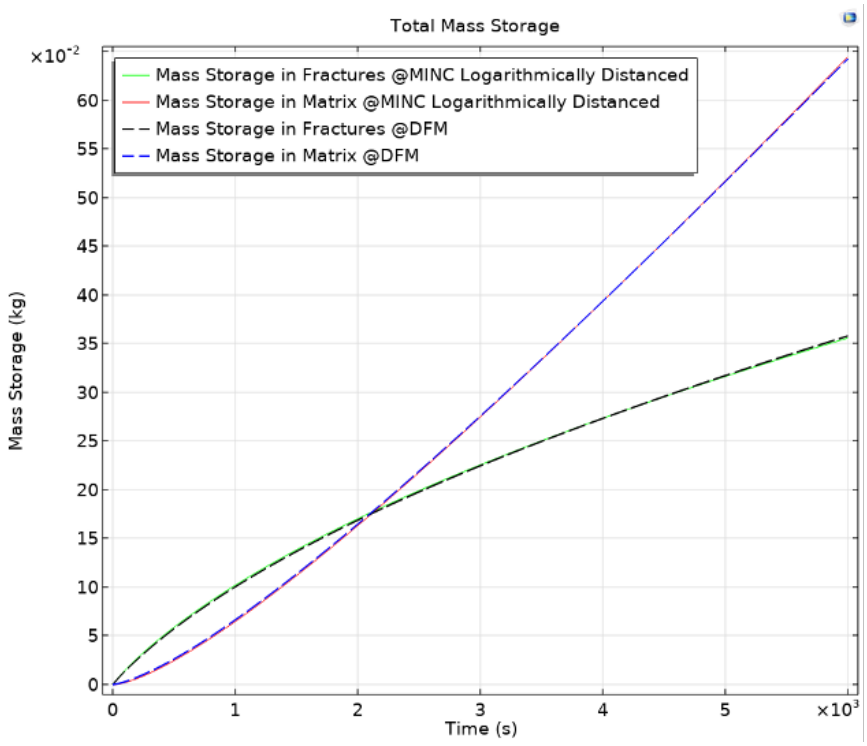

Figure 5.19 Logarithmically distanced method comparison with DFM result

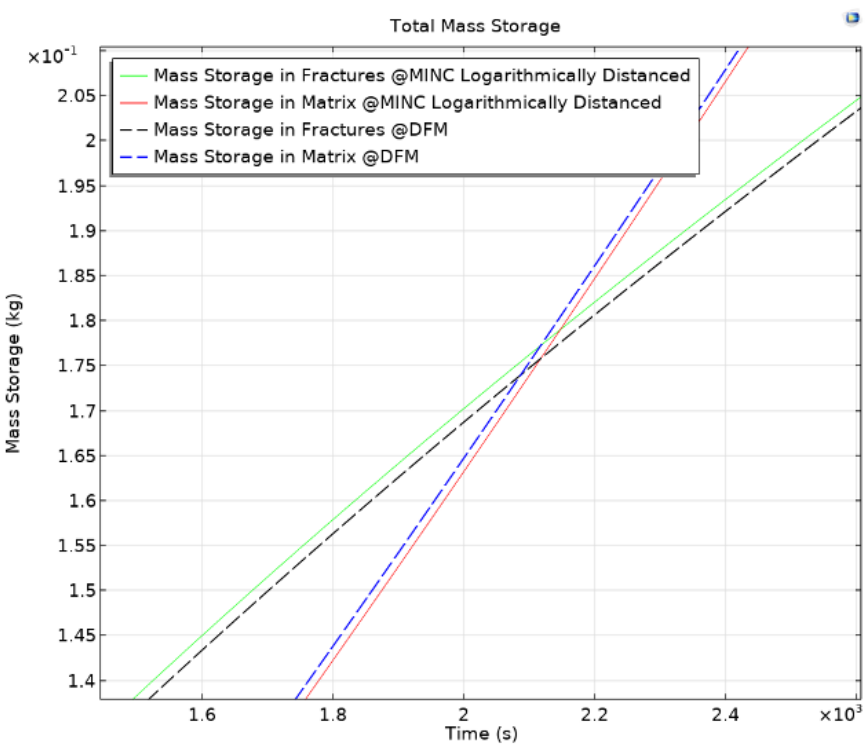

Figure 5.20 Logarithmically distanced method comparison with DFM result - zoomed

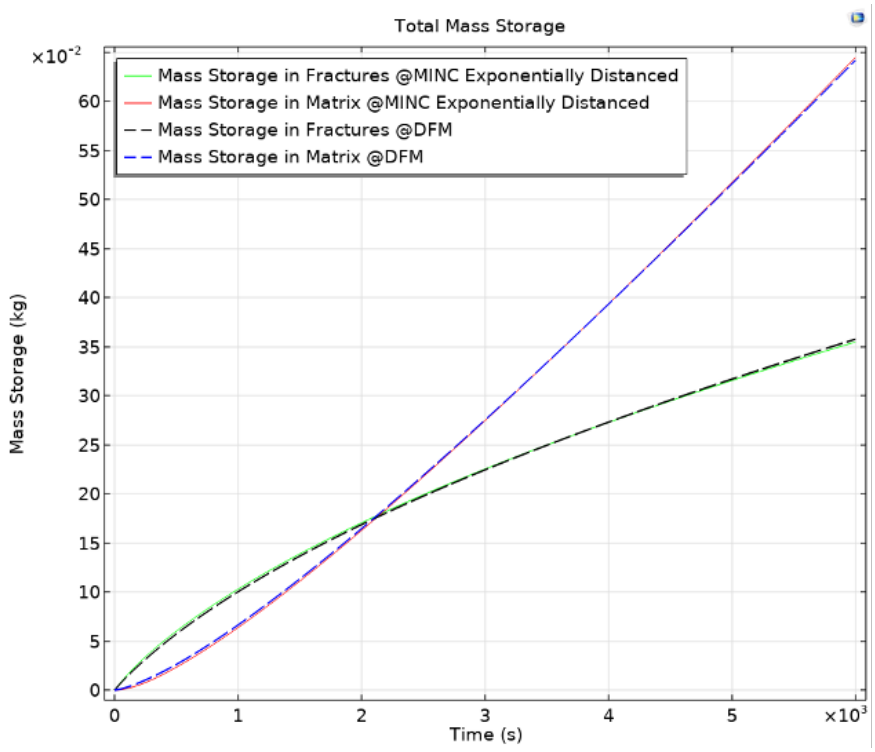

Figure 5.21 Exponentially distanced comparison with DFM result

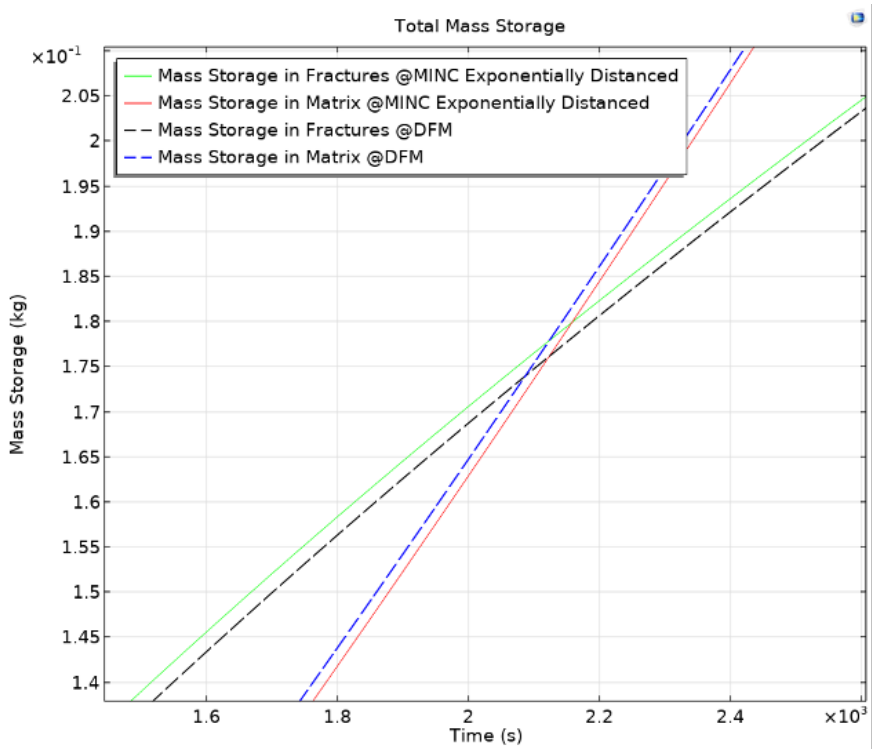

Figure 5.22 Exponentially distanced comparison with DFM result - zoomed

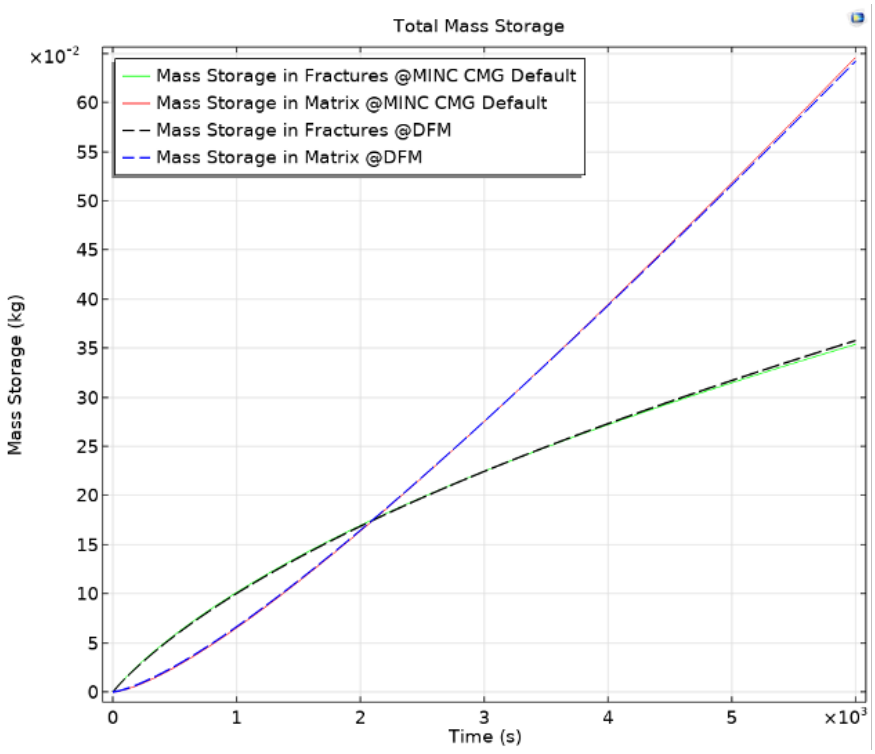

Figure 5.23 Commercial simulator method comparison with DFM result

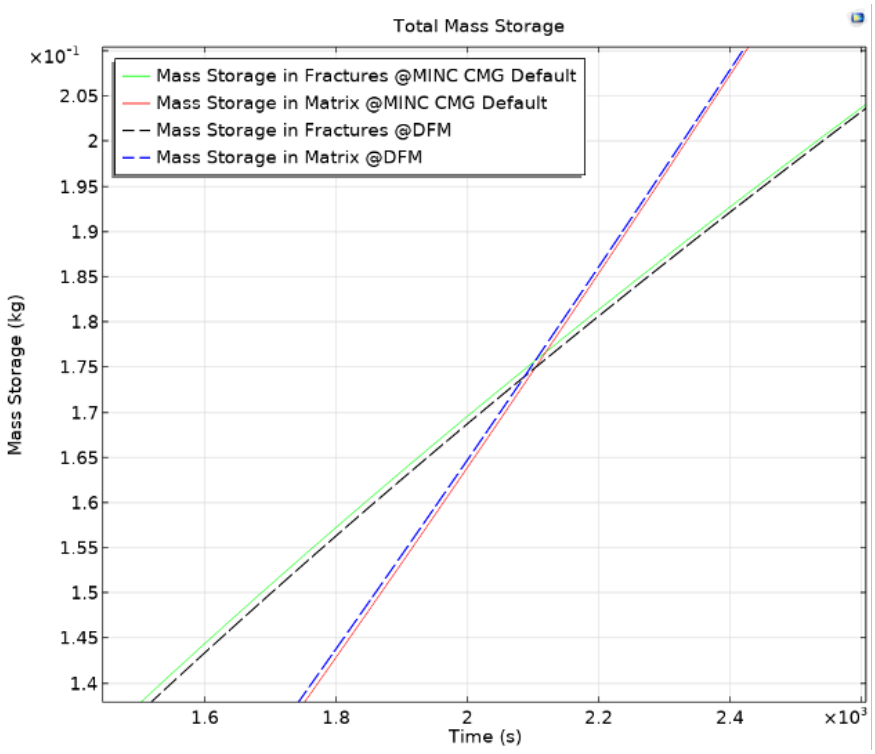

Figure 5.24 Commercial simulator method comparison with DFM result - zoomed

CHAPTER 6

OPTIMIZATION AND RESULT

6.1 Optimization

Optimization has long been in high demand for discovering optimal solutions to a wide range of problems. Physical problems can often be numerically solved using analytical equations. The objective of optimization is to identify the most favorable output that maximizes results while minimizing energy consumption within the system. Numerical optimization processes primarily rely on iterative methods (Hemker & Ciaurri, 2007). The input variables for optimization can encompass various factors, such as the dimensions and shapes of a geometry, as well as material properties. Optimization options include shape optimization, parameter optimization (typically the most commonly used), topological optimization, and more.

6.1.1 Optimization Terminologies

6.1.1.1 Objective Function

In addressing every physical design problem, it is customary to associate it with a figure of merit, often referred to as a cost function or, more commonly, an objective function. Virtually any aspect of the system's performance can be computed through this objective function. The objective is to attain the optimal value for any parameter by either maximizing or minimizing the objective function (Basbug, 2019). The optimal value parameters can govern various aspects of the design, including dimensions, loads, boundary conditions, material properties, and material

distribution. A set of limits and design constraints serves to confine the control variables within certain boundaries.

6.1.1.2 Performance Constraints and Bounds

There might be performance constraints depending on the model solution during system optimization. As an example, it is essential that any constraint parameters must be below a predefined safety limit while minimizing or maximizing the objective function.

Usually, an optimization problem is the need to develop an objective function by changing the control variables inside a set of constraints. The control variables can vary in only the interval of upper and lower bounds (Sinha, 2020).

6.1.1.3 Optimality Tolerance

In all optimization methods, the optimality tolerance plays a crucial role. While it is intended to signify the relative accuracy of the final control variable values, achieving uniform behavior cannot be guaranteed due to significant variations in solver implementations. When the objective function in the last step falls within the optimality tolerance, the iteration comes to a halt.

6.2 Optimization Algorithms

There are two main optimization algorithms:

- Derivative-Free Algorithm
- Gradient-Based Algorithm

These two solver groups are applicable under different conditions with different performance characteristics.

6.2.1 Derivative-Free Algorithm

The origin of Derivative-free algorithms holds on the work of Spendley et al. (1962) and Nelder & Mead (1965). Characteristics of a derivative- or gradient-free algorithm are defined so that the derivative of the objective function with respect to the control variables is not required to compute. Therefore, these methods can suit a wide range of optimization problems (Chong & Żak, 2008). The main advantage of a gradient-free algorithm is that if any discontinuity exists in the objective function, this technique will be efficient and successful during optimization (Hadzic et al., 2011). Even if the problem contains noise or is nonsmoothed, this method can be applicable Specifying geometric dimensions is a common instance of a noisy objective function. When the objective function is evaluated for various control variable values, the geometry changes driven by changing the control variables result in various finite element meshes that impose various discretization errors on the objective function. These solvers do not rely on the objective function pointwise behavior as a decent indicator of the next control variables. That's why derivative-free solvers trust in sampling the objective function at different positions in the control variable space. This method is more robust than a single path and also more expensive.

COMSOL Multiphysics Optimization Module provides five different gradient-free algorithms.

6.2.2 Gradient-Based Algorithms

Implementation of gradient-based, or derivative based, algorithm necessitate the complete vector of the first order derivatives of the objective functions with respect to the discrete gradient of the objective function in the control variable space. These algorithms are efficient because of usage of derivatives of the objective functions. For the gradient-based solvers, the iteration steps in the control variable space, are based on the local derivative calculated in previous points. However, derivative-

based algorithms are not efficient in a local optimum of a problem, convex (Koziel, 2016). This algorithm does not work if any discontinuity exists in the objective function.
COMSOL Multiphysics Optimization Module provides four different gradient-based algorithms.

6.2.3 SNOPT

SNOPT, Sparse Nonlinear Optimizer, was initially developed by Philip E. Gill of the University of California San Diego, and Walter Murray and Michael A. Saunders Stanford University (Gill et al., 2015) which is sequential quadratic programming. SNOPT is, a gradient-based solver available for sparse and large problems. In order to reach the optimum solution, a gradient-based optimization technique is used. Gradients of objective functions or constraints are required and can be computed analytically or numerically.

SNOPT solves a sequence of approximation, meaning that the objective function is introduced as a quadratic polynomial, and the constraints are assumed to be linear (Leyffer & Mahajan, 2011). Sequential quadratic programming is implemented in the fundamental algorithm. Each step in this sequence requires a major or outer iteration, while each approximate quadratic programming problem requires minor and inner iterations.

Optimal results are figured out around corners of a feasible set rather than interior ones with SNOPT method. As a result, the strategy works best for difficulties where there are many active constraints compared to the number of degrees of freedom for the control variable.

6.3 Matrix Permeability Optimization

Two optimization problems are solved in this thesis. The first and most critical one is the determination of matrix permeability for a continuum model based on DFM model. DFM model has $1x10^{-17}$ m^2 matrix permeability and utilizing this value without modification might introduce significant errors during the construction of MINC models. Therefore, Consequently, upscaling this value is essential for the MINC models. Optimization result is expected like in section 5.2.3 where upscaled matrix permeability is explained with the relationship of the interfaces between matrix and fractures. The aim of this optimization is to decide matrix permeability for a MINC representing DFM model. Parameter estimation tool with gradient-based solver, SNOPT, is sufficient to optimize upscaled matrix permeability since there is no constraints or control variables. Optimality tolerance is arranged as 0.0001.

The objective function is minimizing mass storage difference in matrix domain between MINC and DFM model. After a few iterations in COMSOL, matrix permeability for MINC models is optimized as $2.136x10^{-16}$ m^2 (0.216 mD), a value closely approximated by Equation 5.2.

6.4 MINC Parameter Optimization

The other optimization is to decide volume fractions for a MINC model which deviates at least from the DFM model. As discussed before the main function of MINC concept is volume fractions. When volume fractions are changed, meshing i.e., nodal distances, interface areas, and interconnected flow characteristics change directly. Therefore, the aim of optimization is to decide volume fractions for a MINC model which represents the DFM model with the least error.

Fracture volume fraction (f_1) is not optimized since it depends only on the fracture volume in DFM model. The other nine volume fractions are optimized by COMSOL Multiphysics Optimization Module.

It must be noted that the checking parameter is accumulated mass in matrix. While mass storage in matrix is matched, mass storage in fractures is implicitly matched since the total mass storage always must be same for all methods (see Figure 5.14). From the second volume fraction to the tenth one is optimized to decrease the deviation from the mass storage line of DFM.

6.4.1 Optimization Module Steps

Optimization solver is decided as SNOPT, gradient-based, is a strong solver while challenging with many constraints in large scale problem.

The default optimality tolerance decreased to 0.0001 for better accuracy in SNOPT solver. The objective function is minimizing square root of the mass deviance at each time level in matrix domain between DFM and MINC models. The optimization type is set to 'minimize,' aiming to minimize the difference between mass storage in fractures and matrix in DFM model and the mass storage in fractures and matrix in MINC model.

Control variable inputs are, as mentioned before, volume fractions from second one to the last one in the interval 0 and 1. Only one constraint is defined which tells that summation of volume fractions must be equal to 1. Computation time takes approximately 5 minutes.

The output optimized volume fractions values and corresponding MINC parameters are located in Table 6.1.

Table 6.1 Optimized MINC Parameters

Nodes	Volume fractions (f_i)	Nodal Distances ($d_{i,i+1}$)	Interface Areas ($A_{i,i+1}$)
i=1	0.0475	0.020	1.758
i=2	0.0776	0.048	2.734
i=3	0.1020	0.060	3.821
i=4	0.1092	0.055	5.247
i=5	0.0736	0.079	6.145
i=6	0.1600	0.145	6.517
i=7	0.2020	0.157	7.033
i=8	0.1113	0.129	7.483
i=9	0.0685	0.116	7.808
i=10	0.0483		

Mass storage comparison of the optimized MINC model and DFM model is shown in Figure 6.1.

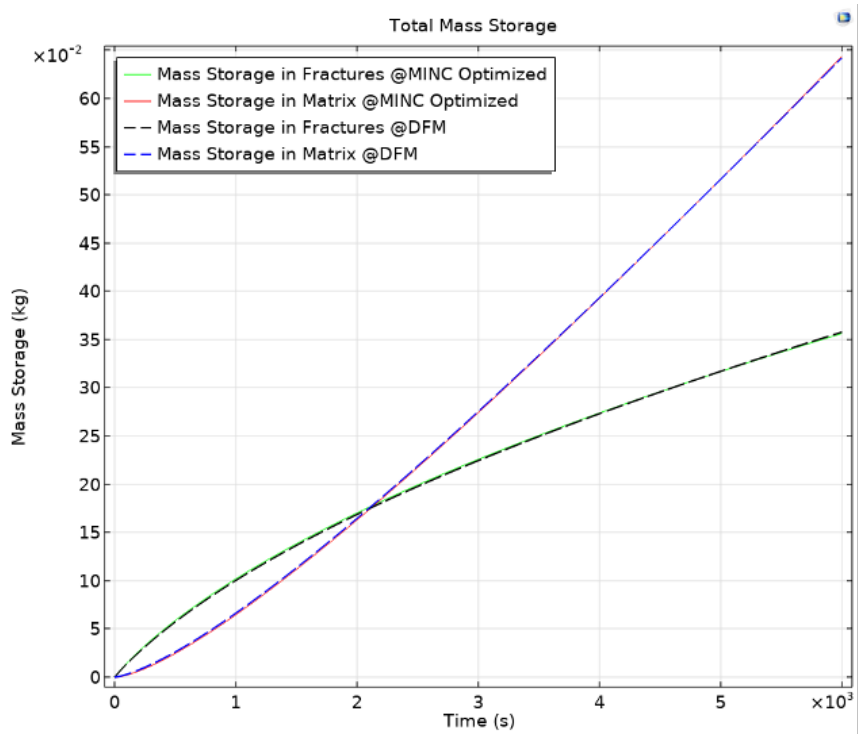

Figure 6.1 Optimized MINC model comparison with DFM result

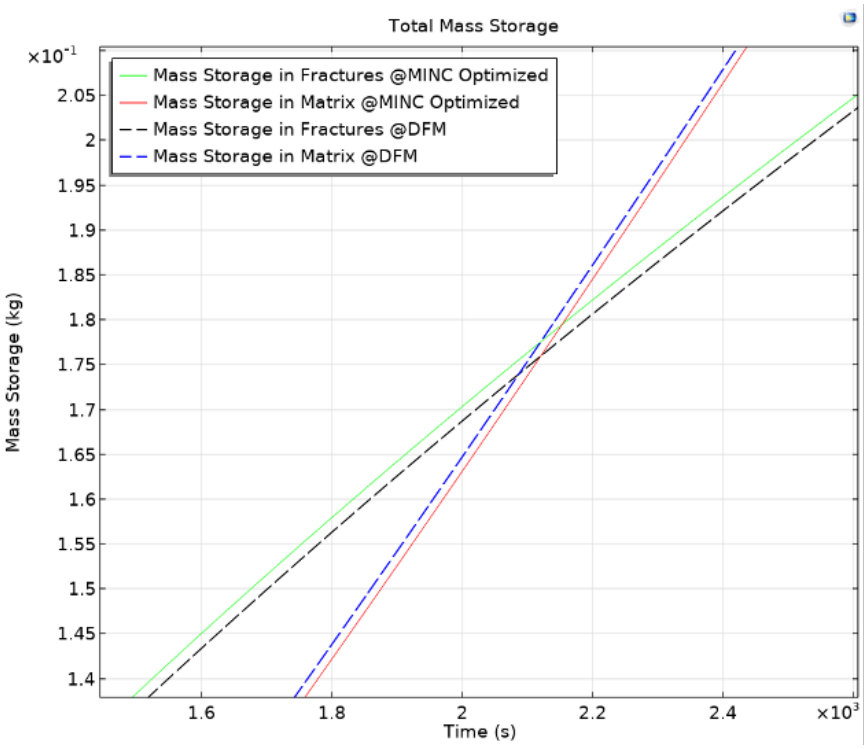

Figure 6.2 Optimized MINC model comparison with DFM result - zoomed

It may not be easily said that the closest line is observed by the optimized MINC model due to blur in the figures. Therefore, deviation of each method from DFM is calculated by the mean squared error method.

6.5 Comparison of MINC Models, Including the Optimized One

6.5.1 Mean Squared Error Calculation

Deciding optimality criteria of a model evaluation is a critical job. The mean squared error of prediction is a valuable parameter to consider when evaluating the quality of a model whose goal is prediction (Wang & Bovik, 2009).

The lower the mean squared error observed, the more closely the data points are dispersed around the reference (mean) data. Inversely, the larger mean squared error indicates that data points are scattered far away from the reference ones.
Mean squared error (MSE) is calculated by the following equation:

$$MSE = \frac{1}{n} \cdot \sum(x_a - x)^2 \tag{6.1}$$

n is the number of sample, x_a is actual data and x is predicted/observed data.

MSE calculations have been performed for three different sets of matrix permeability values. Table 6.2 illustrates the significance of upscaled matrix permeability. A lower error indicates that each MINC model deviates less from the DFM model. When using the upscaled MINC model, the resulting MINC models exhibit the least deviation, as depicted in the fourth column of Table 6.2. The second column indicates a significant error when the matrix permeability is directly used from the DFM model during MINC model creation. In the third column of Table 6.2, MSE is calculated for the MINC models created by using the roughly calculated matrix

permeability from Equation 5.1. It can be inferred that this method is successful in obtaining good results.

Table 6.2 Mean Squared Error

MINC Model Type	MSE (DFM k_m)	MSE (Roughly calculated k_m)	MSE (Optimized k_m)
Equal Volume MINC	3.57E-02	3.62E-06	1.81E-06
Equal Distance MINC	4.39E-02	1.10E-05	8.69E-06
Logarithmically Distanced MINC	3.51E-02	3.87E-06	1.56E-06
Exponentially Distanced MINC	3.78E-02	4.90E-06	3.24E-06
SIMD (CMG) MINC	3.41E-02	1.72E-06	2.54E-06
Optimized MINC	3.50E-02	5.07E-06	1.51E-06

The MINC model with upscaled matrix permeability (located in the last column of Table 6.2) based on optimized volume fractions clearly exhibits the least deviation from the DFM model. Upon closer analysis, it becomes evident that there is minimal deviation in the early time steps, while a strong match is observed in the late time intervals of the solution.

The MINC model that deviates the most from the DFM model is equally distanced MINC model. This deviation occurs because it contradicts the condition outlined by Pruess and Narasimhan (1985), which stipulates that discretization in the vicinity of the fracture continua must be smaller than in the vicinity of the middle of the elementary unit (see Figure 5.9). Moreover, equal volume method obeys that rule automatically since the volume fractions stay constant so that the distances are increasing as getting closer to the innermost element. The second most deviated one is CMG simulator default volume fractions even though nested blocks are much closer around the fracture continuum. In fact, it is expected due to the

underestimation of fracture volume fraction. It can be deduced that this method may be applicable instead of equal distanced method when the fracture volume is not available. Logarithmically and exponentially distanced methods are based on a similar approach during creating computation geometry. However, a considerable difference exists between them, surprisingly.

6.5.2 Computation Time

Table 6.3 shows that MINC models are computed significantly faster compared to DFM model. In other words, the software program requires much more computational power to run DFM model than MINC models. Furthermore, the optimization of volume fractions adds a substantial amount of time to the computation.

Table 6.3 CPU Time Comparison for all Simulation Models

Simulation Method	CPU Time for 4 [m] x 2 [m] part of Bristol Geometry
Equal Volume MINC	a few seconds
Equal Distance MINC	a few seconds
Logarithmically Distanced MINC	a few seconds
Exponentially Distanced MINC	a few seconds
Commercial-simulator-default MINC	a few seconds
Optimized MINC	5 minutes optimization + a few seconds
DFM	~10 minutes

6.6 Comparison of Large-Scale Reservoir MINC Models with Production Well

A large-scale reservoir is created to assess the impact of each MINC method on production. The dimension of the reservoir is 500 [m] x 500 [m]. All reservoir characteristics are same with the previous Bristol geometry MINC models. Mesh of the large-scale reservoir is shown in Figure 6.3 . The mesh of this large-scale reservoir is illustrated in Figure 6.3, consisting of 62500 identical square elementary units, each with dimension of 2 [m] x 2 [m]. Production from the reservoir occurs at a constant rate, originating from the fracture within an elementary unit positioned at the reservoir's edge, as depicted in Figure 6.4 .

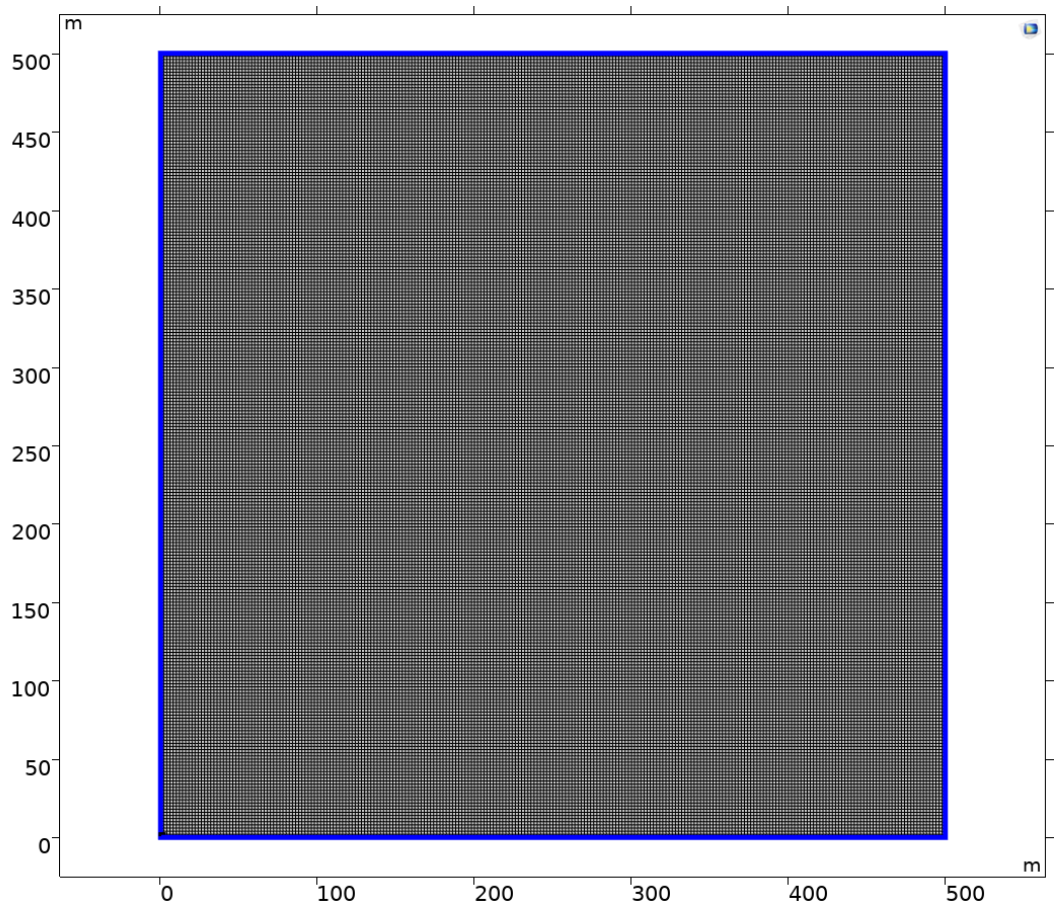

Figure 6.3 Constant source production problem with no flow boundaries - Meshing

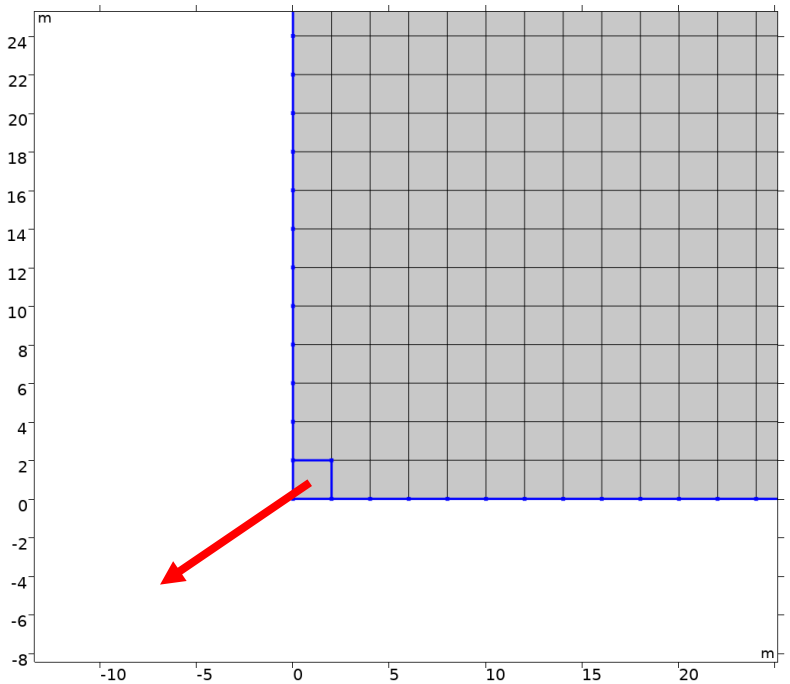

Figure 6.4 Well location of constant source production problem

Methane is continuously extracted 100 kg/min constant rate from the reservoir, which initially has a pressure of $2x10^6$ Pa, over a duration of 6000 seconds. The total mass within the reservoir remains consistent across all models, as the extracted mass is the same. Consequently, the mass within the matrix and fractures is calculated and visualized separately. Specifically, the produced mass from matrix blocks is depicted in a column chart in Figure 6.5 for the first 1000 seconds, providing a detailed comparison of each method's behavior.

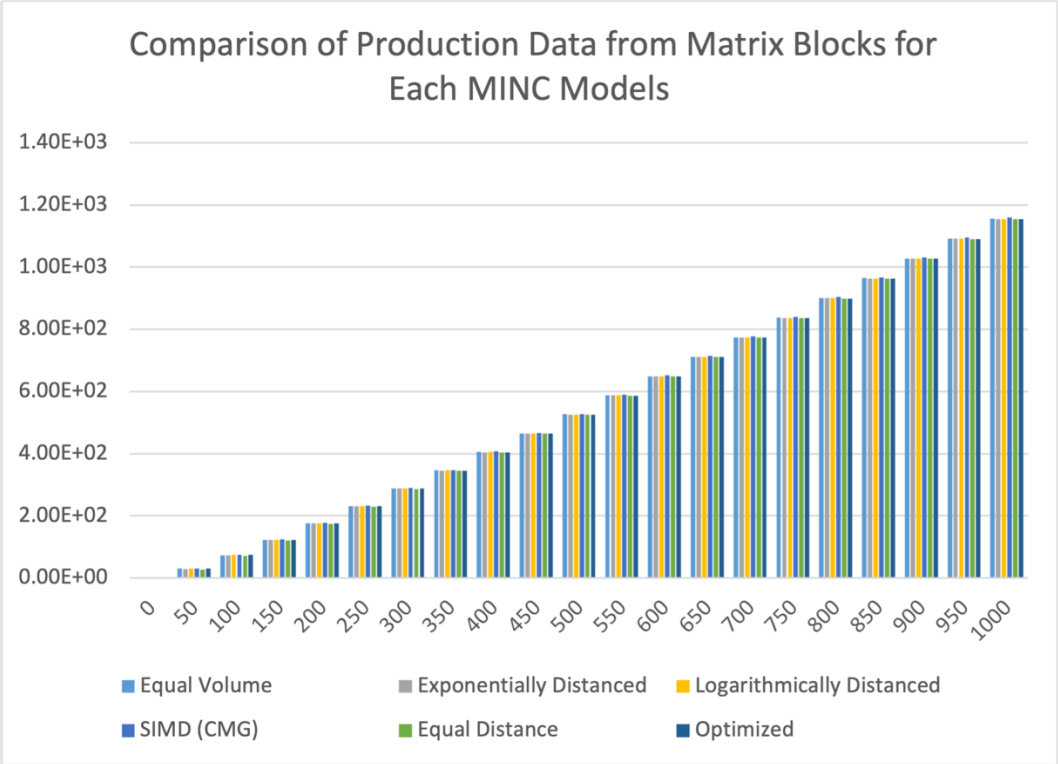

Figure 6.5 Comparison of Production Data from Matrix Blocks for Each MINC Models

As previously mentioned, all methods share the same fracture volume fraction, with the only variation occurring in matrix volume fractions. It can clearly be observed that matrix volume fractions have relatively small impact on the solutions as it can be seen in Figure 6.5 and at the fourth column of Table 6.2. Production from matrix does exhibit slight differences among all the models.

CHAPTER 7

CONCLUSION

This study compares five different MINC models and develops an alternative MINC model to DFM model. MINC models are based on simple nested squared geometry, and the only essential parameters are upscaled permeabilities of fractures, nested matrix elements and volume fractions to compute the model. In contrast, DFM requires the definition of each fracture explicitly. Modeling field-scaled problems with DFM approach is time-consuming and costly. If the whole Bristol geometry (18 [m] x 8 [m]) is computed by DFM model, the computing time is expected to take much more than 15 minutes (current computation time). Parameter optimization is completed for a MINC model by taking DFM as a reference solution. The primary purpose of using DFM model as a reference is that this model is well-known as one of the most accurate models.

Mass storage rate deviation from the DFM model in each time step is the objective function to compare five MINC models with DFM. Each reservoir has its own particular volume fractions. However, different MINC models have revealed that volume fractions do not affect the solution significantly contrary to expectations when upscaled matrix permeability is determined. In addition, same volume fractions are employed to construct large-scale reservoir and it is observed that matrix volume fractions have only a slight effect on the results. Also, in cases where there is insufficient time for upscaling, approximating matrix permeability from the Darcy's Law relationship between two models significantly provides convenience to obtain good results.

The best representative MINC model is constructed by optimizing volume fractions and deciding true matrix permeability for a specific part of the Bristol Channel. The

distribution of fracture network in Bristol geometry is accepted as homogeneous and well-connected to model with MINC approach. Therefore, the optimized matrix permeability and volume fractions can be applicable to the whole reservoir. If the entire Bristol geometry is computed with the optimized parameters, it is not expected to exceed 5 minutes computation time. With the optimized MINC model, computation time, cost, and pre-processing efforts will be saved significantly, and the model would be as accurate as the DFM model when considered on the same scale.

REFERENCES

Ahmed, T. (2010). Chapter 17 - Fractured Reservoirs. In T. Ahmed (Ed.), *Reservoir Engineering Handbook (Fourth Edition)* (pp. 1338–1432). Gulf Professional Publishing. https://doi.org/https://doi.org/10.1016/B978-1-85617-803-7.50025-0

Basbug, S. (2019). An Antenna Design Technique Based on Differential Evolution Algorithm Using An Objective Function Designed with Finite Element Method Simulations. *2019 IEEE 13th International Conference on Application of Information and Communication Technologies (AICT)*, 1–4.

Batchelor, G. K. (2000). An Introduction to Fluid Dynamics. In *Cambridge Mathematical Library*. Cambridge University Press. https://doi.org/DOI: 10.1017/CBO9780511800955

Billaux, D., Chiles, J. P., Hestir, K., & Long, J. (1989). Three-dimensional statistical modelling of a fractured rock mass—an example from the Fanay-Augères mine. *International Journal of Rock Mechanics and Mining Sciences & Geomechanics Abstracts*, *26*(3), 281–299. https://doi.org/https://doi.org/10.1016/0148-9062(89)91977-3

Bourbiaux, B., Granet, S., Landereau, P., Noetinger, B., Sarda, S., & Sabathier, J. C. (1999). *Scaling Up Matrix-Fracture Transfers in Dual-Porosity Models: Theory and Application*.

Chen, M., Hosking, L. J., Sandford, R. J., & Thomas, H. R. (2020). A coupled compressible flow and geomechanics model for dynamic fracture aperture during carbon sequestration in coal. *International Journal for Numerical and Analytical Methods in Geomechanics*, *44*(13), 1727–1749. https://doi.org/10.1002/nag.3075

Chong, E. K. P., & Żak, S. H. (2008). *An Introduction to Optimization: Chong/An Introduction*. https://api.semanticscholar.org/CorpusID:63762986
citations-20230824T002120. (n.d.).

Coats, K. H. (1999). *SPE SPE 18427 Implicit Compositional Simulation of Single-Porosity and Dual-Porosity Reservoirs*. http://onepetro.org/spersc/proceedings-pdf/89RS/All-89RS/SPE-18427-MS/3215835/spe-18427-ms.pdf/1

Egya, D. O. (2018). *Characterisation of naturally fractured reservoirs using geological well-testing*.

Ermakova, E., Elberdov, T., & Rynkovskaya, M. I. (2022). Shape Optimization of a Shell in Comsol Multiphysics. *Comput.*, *10*, 54.

Farah, N., Ding, D. Y., & Delorme, M. (2016). Extension of the multiple interacting continua method to discrete fracture models for unconventional low permeability reservoir simulations. *SPE/AAPG/SEG Unconventional Resources Technology Conference 2016*. https://doi.org/10.15530/urtec-2016-2443586

Gill, P. E., Wong, E., Murray, W., & Saunders, M. A. (2015). *User's Guide for SNOPT Version 7.4: Software for Large-Scale Nonlinear Programming*.

Hadzic, Fedja., Tan, Henry., & Dillon, T. S. (2011). *Mining of data with complex structures*. Springer-Verlag.

Hassanzadeh, H., & Pooladi-Darvish, M. (2006). Effects of fracture boundary conditions on matrix-fracture transfer shape factor. *Transport in Porous Media*, *64*(1), 51–71. https://doi.org/10.1007/s11242-005-1398-x

Hemker, P. W., & Ciaurri, D. E. (2007). A trust-region strategy for manifold-mapping optimization. *J. Comput. Phys.*, *224*, 464–475.

Hull, L. C., & Clemo, T. M. (1987). *Effects of using a continuum representation of discrete fracture networks*.

Jiang, J., & Younis, R. M. (2016). Hybrid coupled discrete-fracture/matrix and multicontinuum models for unconventional-reservoir simulation. *SPE Journal*, *21*(3), 1009–1027. https://doi.org/10.2118/178430-PA

Karimi-Fard, M., Gong, B., & Durlofsky, L. J. (2006). Generation of coarse-scale continuum flow models from detailed fracture characterizations. *Water Resources Research*, *42*(10). https://doi.org/10.1029/2006WR005015

Kazemi, H., & Gilman, J. R. (1993). *6 – Multiphase Flow in Fractured Petroleum Reservoirs*.

Kazemi, H., Merrill, L. S., Porterfield, K., & Zeman, P. (1976). NUMERICAL SIMULATION OF WATER-OIL FLOW IN NATURALLY FRACTURED RESERVOIRS. *Society of Petroleum Engineers Journal*, *16*, 317–326.

Koziel, S. (2016). Computational Optimization, Methods and Algorithms. *Computational Optimization, Methods and Algorithms*.

Kuchuk, F., Biryukov, D., & Fitzpatrick, T. (2014). *Fractured Reservoir Modeling and Interpretation*.

Lee, S. H., Lough, M. F., & Jensen, C. L. (2001). Hierarchical modeling of flow in naturally fractured formations with multiple length scales. *Water Resources Research*, *37*(3), 443–455. https://doi.org/10.1029/2000WR900340

Lei, Q., Latham, J.-P., & Tsang, C.-F. (2017). The use of discrete fracture networks for modelling coupled geomechanical and hydrological behaviour of fractured rocks. *Computers and Geotechnics*, *85*, 151–176. https://doi.org/https://doi.org/10.1016/j.compgeo.2016.12.024

Leyffer, S., & Mahajan, A. (2011). *Software for Nonlinearly Constrained Optimization*. https://api.semanticscholar.org/CorpusID:124868051

Li, L., & Lee, S. H. (2008). *Efficient Field-Scale Simulation of Black Oil in a Naturally Fractured Reservoir Through Discrete Fracture Networks and Homogenized Media*. http://onepetro.org/REE/article-pdf/11/04/750/2545183/spe-103901-pa.pdf/1

Lim, K. T., & Aziz, K. (1995). Matrix-fracture transfer shape factors for dual-porosity simulators. *Journal of Petroleum Science and Engineering*, *13*, 169–178.

Liu, J., Wang, J. G., Gao, F., Leung, C. F., & Ma, Z. (2019). A fully coupled fracture equivalent continuum-dual porosity model for hydro-mechanical process in fractured shale gas reservoirs. *Computers and Geotechnics*, *106*, 143–160. https://doi.org/https://doi.org/10.1016/j.compgeo.2018.10.017

Mayerhofer, M. J., Lolon, E. P., Youngblood, J. E., & Heinze, J. R. (2006). *Integration of Microseismic-Fracture-Mapping Results With Numerical Fracture Network Production Modeling in the Barnett Shale*.

Moinfar, A., Varavei, A., Sepehrnoori, K., & Johns, R. T. (n.d.). *Development of a Coupled Dual Continuum and Discrete Fracture Model for the Simulation of Unconventional Reservoirs*. http://onepetro.org/spersc/proceedings-pdf/13RSS/All-13RSS/SPE-163647-MS/1562126/spe-163647-ms.pdf/1

Mora, C. A., & Wattenbarger, R. A. (2006). Analysis and Verification of Dual Porosity and CBM Shape Factors. *Journal of Canadian Petroleum Technology*, *48*, 17–21. https://api.semanticscholar.org/CorpusID:129039654

Narasimhan, T. N., & Witherspoon, P. A. (1978). Numerical model for saturated-unsaturated flow in deformable porous media: 3. Applications. *Water Resources Research*, *14*, 1017–1034.

Nelder, J. A., & Mead, R. (1965). A Simplex Method for Function Minimization. *Comput. J.*, *7*, 308–313.

Peñuela, G., Civan, F., Hughes, R. G., & Wiggins, M. L. (2002). *Time-Dependent Shape Factors for Interporosity Flow in Naturally Fractured Gas-Condensate Reservoirs*.

Powell, M. J. D. (1994). *A Direct Search Optimization Method That Models the Objective and Constraint Functions by Linear Interpolation*.

Powell, M. J. D. (2009). *The BOBYQA algorithm for bound constrained optimization without derivatives*.

Pruess, K. (1992). *Brief Guide to the MINC-Method for Modeling Flow and Transport in Fractured Media*.

Pruess, K. (1983). GMINC - A MESH GENERATOR FOR FLOW SIMULATIONS IN FRACTURED RESERVOIRS. *Lawrence Berkeley National Laboratory*.

Pruess, K., & Karasaki, K. (1982). *Proximity functions for modeling fluid and heat flow in reservoirs with stochastic fracture distributions*.

Pruess, K., & Narasimhan, T. N. (1982). On fluid reserves and the production of superheated steam from fractured, vapor-dominated geothermal reservoirs. *Journal of Geophysical Research*, *87*, 9329–9339.

Pruess, K., & Narasimhan, T. N. (1985). A PRACTICAL METHOD FOR MODELING FLUID AND HEAT FLOW IN FRACTURED POROUS MEDIA. *Society of Petroleum Engineers Journal*, *25*, 14–26.

Ren, G., Jiang, J., & Younis, R. M. (2017). *SPE-182726-MS Fully-Coupled XFEM-EDFM Hybrid Model for Geomechanics and Flow in Fractured Reservoirs*. http://onepetro.org/spersc/proceedings-pdf/17RSC/3-17RSC/D031S010R003/1298308/spe-182726-ms.pdf/1

Rostami, P., Sharifi, M., & Dejam, M. (2020). Shape factor for regular and irregular matrix blocks in fractured porous media. *Petroleum Science*, *17*(1), 136–152. https://doi.org/10.1007/s12182-019-00399-9

Sarda, S., Jeannin, L., & Bourbiaux, B. (2002). *Hydraulic Characterization of Fractured Reservoirs: Simulation on Discrete Fracture Models*.

Sinha, G. R. (2020). *Modern Optimization Methods for Science, Engineering and Technology*. https://api.semanticscholar.org/CorpusID:209789501

Spendley, W., Hext, G. R., & Himsworth, F. R. (1962). Sequential Application of Simplex Designs in Optimisation and Evolutionary Operation. *Technometrics*, *4*, 441–461.

Svanberg, K. (1987). The method of moving asymptotes—a new method for structural optimization. *International Journal for Numerical Methods in Engineering*, *24*, 359–373.

Svanberg, K. (2013). *MMA and GCMMA-two methods for nonlinear optimization*.

Tatomir, A. B. (2012). *From discrete to continuum concepts of flow in fractured porous media*.

Tsang, Y. W., & Tsang, C. F. (n.d.). *Lawrence Berkeley National Laboratory Recent Work Title CHANNEL MODEL OF FLOW THROUGH FRACTURED MEDIA Permalink https://escholarship.org/uc/item/9jv3w5nx Publication Date*.

Wächter, A., & Biegler, L. T. (2005). Line Search Filter Methods for Nonlinear Programming: Motivation and Global Convergence. *SIAM J. Optim.*, *16*, 1–31.

Wang, Z., & Bovik, A. C. (2009). Mean squared error: Love it or leave it? A new look at Signal Fidelity Measures. *IEEE Signal Processing Magazine*, *26*, 98–117.

Warren, J. E., & Root, P. J. (1963). The Behavior of Naturally Fractured Reservoirs. *Society of Petroleum Engineers Journal*, *3*, 245–255.

Witherspoon, P. A., Wang, J. S. Y., Iwai, K., & Gale, J. E. (1979). *Validity of cubic law for fluid flow in a deformable rock fracture. Technical information report No. 23*.

Wu, Y. S., Li, J., Ding, D. Y., Wang, C., & Di, Y. (2014). A generalized framework model for the simulation of gas production in unconventional gas reservoirs. *SPE Journal*, *19*(5), 845–857. https://doi.org/10.2118/163609-PA

Xue, X., Yang, C., Onishi, T., King, M. J., & Datta-Gupta, A. (2019). Modeling hydraulically fractured shale wells using the fast-marching method with local grid refinements and an embedded discrete fracture model. *SPE Journal*, *24*(6), 2590–2608. https://doi.org/10.2118/193822-PA

Yang, D., Xue, X., & Chen, J. (2018). *SPE-190096-MS High Resolution Hydraulic Fracture Network Modeling Using Flexible Dual Porosity Dual Permeability Framework* (Vol. 2). http://onepetro.org/SPEWRM/proceedings-pdf/18WRM/5-18WRM/D051S015R001/1237049/spe-190096-ms.pdf/1

Zimmerman, R. W., Bodvarsson, G. S., & Bodvarsson, G. S. (1994). *Hydraulic Conductivity of Rock Fractures*.

APPENDICES

A. MATLAB CODE – Proximity Function

```
Ad %clc ;
clear all;
%Begin Input
n_minc_cont=10;%number of minc continua
dim=2; %element dimension for 2D
n_f_p=2; %number of perpendicular fracture plane sets
frac_ap=0.048100925; % fracture aperture m
V_actual=8; % 3D volume of discretized element m^3
V_0=V0_function(dim,V_actual);% depending on dime 2,3 discretized element
volume is modified
dx_frac=2; %fracture spacing in x m
dy_frac=2; %fracture spacing in y m
dz_frac=2; %fracture spacing in z m
f=zeros(1,n_minc_cont); % for the constant volume method with fractions (N=10)
f(1)=Proximity(n_f_p,frac_ap/2,dx_frac,dy_frac,dz_frac); %volume fraction of
fracture
f(2)=0.105830833333333;
f(3)=0.105830833333333;
f(4)=0.105830833333333;
f(5)=0.105830833333333;
f(6)=0.105830833333333;
f(7)=0.105830833333333;
f(8)=0.105830833333333;
f(9)=0.105830833333333;
```

```
f(10)=1-f(1)-f(2)-f(3)-f(4)-f(5)-f(6)-f(7)-f(8)-f(9);% volume fraction of inner most
domain
%End Input
P=zeros(1,n_minc_cont);% proximity function value
x=zeros(1,n_minc_cont-1);% x values for given proximity function value
V=zeros(1,n_minc_cont);% MINC volumes with V1 fracture volume
d_intf=zeros(1,n_minc_cont-1);
A_intf=zeros(1,n_minc_cont-1);
dx_m=dx_frac-frac_ap; % matrix spacing in x m
dy_m=dy_frac-frac_ap; % matrix spacing in y m
dz_m=dz_frac-frac_ap; % matrix spacing in z m

for i = 2 : n_minc_cont-1
   sum_f=0;
   for n=2:i
      sum_f=sum_f+f(n);
   end
   P(i)= sum_f/(1-f(1));
   % calculate x by iteration and proximity function objective
   LB=1e-6;%lower bound of x
   d_spacing = [dx_m,dy_m,dz_m];
   UP=min(d_spacing)/2; % upperbound
   cost = @(x_cost,i) abs(P(i)-Proximity(n_f_p,x_cost,dx_m,dy_m,dz_m));
   objectivefcn = @(x_ob,varargin) cost(x_ob,i);
   %options = optimset('PlotFcns','optimplotfval','TolX',1e-
10,'MaxFunEvals',1000,'MaxIter',1000);
   options =
optimset('PlotFcns','optimplotfval','FunValCheck','on','MaxFunEvals',10000000,'M
axIter',100000,'TolX',1e-10,'TolFun',1e-10);
   x0=1e-16;
```

```
    [x(i), fval, exitflag] = fminsearchbnd(objectivefcn,x0,LB,UP,options);
end

% Most inner block calculations acc. to Warren Root
ui=dx_m-2*x(n_minc_cont-1);
vi=dy_m-2*x(n_minc_cont-1);
wi=dz_m-2*x(n_minc_cont-1);
if (n_f_p ==3)
    l= 3*ui*vi*wi/(ui*vi+vi*wi+ui*wi);
    d_inner=l/10;
else
    if (n_f_p ==2)
        l=2*ui*vi/(ui+vi);
        d_inner=l/8;
    else
        if(n_f_p ==1)
            l=ui;
            d_inner=l/6;
        end
    end
end

% Minc Volumes
for i = 1 : n_minc_cont
V(i)= f(i)*V_0;
end

% distance between the blocks
% 1 is fracture domain, ex: d_intf(1) means d_1_2, d_intf(2) means d_2_3
d_intf(1)=0+(x(2)-x(1))/2;
```

```
for i = 2 : n_minc_cont-2
d_intf(i)= (x(i)-x(i-1))/2 + (x(i+1)-x(i))/2;
end
d_intf(n_minc_cont-1)= (x(n_minc_cont-1)-x(n_minc_cont-2))/2 + d_inner;

% Area between the blocks ex: A_intf(1) means A_1_2, A_intf(2) means A_2_3
delta_x=1e-10;
for i = 1 : n_minc_cont-1
%dP/dx
dP= Proximity(n_f_p,x(i)+delta_x,dx_m,dy_m,dz_m)-
Proximity(n_f_p,x(i),dx_m,dy_m,dz_m);
A_intf(i)=(1-f(1))*V_0*dP/delta_x;
end

function proxm= Proximity(n_f_p,x,dx_spacing,dy_spacing,dz_spacing)
u=2*x/dx_spacing;
v=2*x/dy_spacing;
w=2*x/dz_spacing;
d_spacing = [dx_spacing,dy_spacing,dz_spacing];
if (n_f_p ==3)
   if (2*x < min(d_spacing))
      proxm = u+v+w-u*v-v*w-u*w+u*v*w;
   else
      proxm = 1;
   end
else
   if (n_f_p ==2)
      if (2*x < min(d_spacing))
         proxm=u+v-u*v;
      else
```

```
            proxm = 1;
        end

    else
        if(n_f_p==1)
            if (2*x < min(d_spacing))
                proxm=u;
            else
                proxm = 1;
            end

        end
    end
end
end

function v0 = V0_function(dimension,V_act)
    if (dimension ==3)
        v0= V_act;
    else
        if (dimension ==2)
            v0=(V_act^(1/3))^2;
        else
            if(dimension==1)
                v0=(V_act^(1/3));
            end
        end
    end
end
```

B. Derivative-Free Algorithms

Coordinate search Method

The goal of the coordinate search solver is to improve the objective function through the coordinate directions of the control parameters space. The lengths of space are increased or decreased for appropriate values of the objective function. This solver interprets the gradients of objective function indirectly. That's because gradients may not be supplied as a quantity directly in some conditions.

Monte Carlo Method

The Monte Carlo solver assigns points randomly by uniform distribution within a box where an upper bound and a lower bound are compulsory. This solver is successful in gaining statistical information of design changes after examining the range of values which are taken by the objective function. On the other hand, it's slow to complete the optimal value because of looking for the all-range space specified by the parameter bounds. Rather than the other optimization algorithms implemented in COMSOL, Monte Carlo method is looking for the minima both locally and globally.

Nelder–Mead Method

The Nelder Mead method was initially introduced by Spendley, Hext, and Himsworth in 1962 and developed by Nelder and Mead (1965). The technique holds on an ordinary procedure, simplex, which is a geometric shape, is concluded by n+1 (n= a number of control variables) points in the n dimensional space (Chong & Żak, 2008). The worst point of a simplex in the control variable space is exchanged by using reflections, expansions, and contractions iteratively to recover the objective function.

BOBYQA

The name BOBYQA means Bound Optimization by Quadratic Approximation. A quadratic model, valid in a trust region, approximates the objective function values by iteration. The number of interpolations is fixed to two times the number of control variables plus one (Powell, 2009).

COBYLA

The name COBYLA is the abbreviation of Constrained Optimization by Linear Approximation. This is another derivative free iterative approach that linear approximation sequence is formed by each iteration at the vertices of a simlex in a trust region. The COBYLA technique is applicable for small problems since linear approximation can be inadequate for the high number variables. (Powell, 1994).

C. Gradient-Based Algorithms

IPOPT

IPOPT, interior Point Optimizer, is one of the gradient-based optimization solver techniques which is based on a line search filter interior- point algorithm (Wächter & Biegler, 2005) . IPOPT is available for large-scale nonlinear problems with many or difficult constraints to reach optimal solution. Analytical or semi-numerical computation are externally necessary for the gradients of both the objective function and all constraints. IPOPT is focused on linear system solutions, problem function computations, and derivatives of problem functions (Ermakova et al., 2022).

MMA

MMA, Method of Moving Asymptotes, was created by Svanberg (1987) and has the ability to compute every type of optimization problem primarily available to the enormous number of control variables. In basic terms, MMA is a linear process rather than approximating second-order information about the objective function. Its sub-problems are linear approximations of the original problem, but they also contain contributions from rational functions that resemble barriers and are governed by moving asymptotes. Nothing but the asymptotes' present position is stored between outer iterations regarding the problem (Svanberg, 2013).

Levenberg – Marquardt Method

The Levenberg-Marquardt only employs least-squares-type objective functions. Constraints are not validated by this method. This method often converges more quickly than SNOPT, IPOPT, or MMA for problems of least-squares type since it is designed exclusively for addressing them. The technique uses first-order derivatives to compute second-order derivatives during least squares fitting.

The evaluation of an approximate Hessian and regularization of the Hessian approximation are the two main concepts that underlie the Levenberg-Marquardt algorithm. Since a Newton iteration can theoretically be performed directly using an approximate Hessian (matrix of second derivatives), the specific structure of least-squares objective functions makes this possible in a cost-efficient way. However, the Newton process could be more stable since least-squares issues are frequently unconstrained. In order to ensure the Hessian's positive definiteness, a regularization parameter is included. Based on the outcome of the previous phase, this parameter is updated by iterations. (Madsen et. al., 2004).